Chemical Geology 335 (2013) 172–188

Contents lists available at SciVerse ScienceDirect

Chemical Geology

journal homepage: www.elsevier.com/locate/chemgeo

Mobility and chemical fate of antimony and arsenic in historic mining environments of the Kantishna Hills district, Denali National Park and Preserve, Alaska

Vanessa J. Ritchie [a,b], Anastasia G. Ilgen [b,1], Seth H. Mueller [c], Thomas P. Trainor [b,*], Richard J. Goldfarb [d]

[a] Fairbanks Environmental Services, Inc., 3538 International Street, Fairbanks AK 99701, United States
[b] Department of Chemistry and Biochemistry, University of Alaska Fairbanks, P.O. Box 756160, Fairbanks AK 99775, United States
[c] Boliden Mineral AB, Kontorsvägen 1, SE-936 81 Boliden, Sweden
[d] US Geological Survey, P.O. Box 25046, Mail Stop 973, Denver Federal Center, Lakewood, CO 80225, United States

ARTICLE INFO

Article history:
Received 5 April 2012
Received in revised form 2 October 2012
Accepted 4 October 2012
Available online 12 October 2012

Editor: J. Fein

Keywords:
Antimony
Arsenic
Hydrogeochemistry
Alaska
Denali Park

ABSTRACT

The Kantishna Hills mining district of interior Alaska, USA, located within Denali National Park and Preserve, contains a number of antimony lode deposits, including Alaska's historically largest antimony producer, the Stampede mine. Oxidative weathering of sulfidic tailings and waste rock associated with historic mining operations has impacted water quality in the region. In the Stampede and Slate Creek watersheds, antimony and arsenic concentrations in stream waters were as high as 720 μg/L and 239 μg/L, respectively. Antimony in all water samples is predominantly present as Sb(V), whereas arsenic was detected in varying ratios of As(III) and As(V). Based on X-ray absorption spectroscopy (XAS) measurements reduced As(III) and Sb(III) were identified in mine waste materials, whereas predominantly oxidized forms, As(V) and Sb(V), were found in downstream sediments. Elevated antimony concentrations extend for more than 8 km downstream from the antimony lodes, whereas arsenic quickly attenuates within 1.5 km. The difference between antimony and arsenic aqueous phase speciation suggests that antimony oxidation is more rapid than arsenic within this system. A high correlation is observed between antimony, arsenic, and iron concentrations in fine-fraction streambed sediments downstream of the source lodes. This suggests that sorption and co-precipitation with iron (hydr)oxides are important pathways for the attenuation of antimony and arsenic in these interior Alaska watersheds. Further XAS characterization of the downstream sediments corroborates these observations and indicates that antimony is adsorbed to Fe-oxide phases as inner-sphere bi-dentate edge and corner sharing complexes. The trace element redox states, as well as downstream partitioning, are mainly controlled by iron speciation based on the strong correlation between redox potentials calculated from iron (Fe(II)/Fe(III)) and arsenic (As(III)/As(V)).

1. Introduction

Oxidative weathering of acid-forming sulfide minerals, such as pyrite (FeS_2), and associated arsenopyrite (FeAsS) and stibnite (Sb_2S_3), has the potential to impact water quality. Within interior Alaska, there are a number of examples of anomalous aqueous concentrations of arsenic (As) and antimony (Sb), as much as hundreds of μg/L, associated with both natural undeveloped metallic mineral occurrences and legacy mining operations (Mueller et al., 2004, 2010). Such elevated concentrations are potentially harmful to aquatic ecosystems (Vaughan, 2006; Nam et al., 2009) and fall well above the USEPA maximum contaminant levels (MCLs) in drinking water of 10 and 6 μg/L for arsenic and antimony, respectively. The fate of trace elements such as arsenic and antimony in acid drainage waters is influenced by a variety of processes including acid neutralization, secondary mineral precipitation, aqueous complexation, and sorption onto particles and colloids within the water column or streambed sediments. Neutralization, through dissolution of carbonate or aluminosilicate minerals, or by dilution with ground or surface water, will dramatically reduce the solubility of some metal ions, such as Fe(III), causing formation of crystalline and amorphous precipitates that serve as sinks for trace constituents (Stumm and Morgan, 1996; Nordstrom and Alpers, 1999). The concentrations of metals such as Cd, Cu, Ni, Pb and Zn, and metalloids such as As and Sb, are mainly controlled by their sorption or co-precipitation to particulates and colloids of the secondary phases (e.g., amorphous ferric-hydroxide or ferrihydrite, $Fe(OH)_3$) or other high surface area materials. The colloidal and fine-grained sorbents can be transported long distances before settling to the streambed, serving as a significant transport vector for trace elements from the source regions (Smith et al., 1992, 1993; Plumlee et al., 1999; Smith, 1999). Therefore, one of the key factors in considering the impact of sulfide oxidation and dissolution on water quality is the extent to which the metal(loids) partition between solution and solid phases, which in turn is strongly influenced by the solution speciation.

* Corresponding author.
E-mail address: tptrainor@alaska.edu (T.P. Trainor).
[1] Current address: Sandia National Laboratories, P.O. Box 5800 MS-0754 Albuquerque, New Mexico 87185, United States.

0009-2541/$ – see front matter © 2012 Elsevier B.V. All rights reserved.
http://dx.doi.org/10.1016/j.chemgeo.2012.10.016

Upon exposure to surface conditions, arsenic (Courtin-Nomade et al., 2009; Klimko et al., 2011) and antimony (Klimko et al., 2011) associated with sulfide-rich ores are quickly oxidized. In surface soil and aquatic environments, arsenic and antimony most commonly exist in either the +3 or +5 oxidation state in the form of oxyanions. It has generally been observed that As(III) has a lower affinity for binding to mineral surfaces and is found to be more mobile in aquatic systems than As(V) (Zobrist et al., 2000; Smedley and Kinniburgh, 2002; Herbel and Fendorf, 2006). At acidic to circum-neutral pH, As(V) is effectively immobilized by sorption and co-precipitation with Fe-, Al-, and Mn-(hydr)oxides (Courtin-Nomade et al., 2009). With increasing pH to values above 8.5, adsorbed arsenic is mobilized from oxide surfaces (Smedley and Kinniburgh, 2002; Bissen and Frimmel, 2003). Both As(V) and As(III) can be released from metal (hydr)oxides during the onset of strongly reducing conditions due to the reductive dissolution of the sorbent (Guo et al., 1997; Langner and Inskeep, 2000; Smedley and Kinniburgh, 2002; Takahashi et al., 2004; Herbel and Fendorf, 2006). Microbial reduction of sorbed arsenic has also been suggested to trigger release of arsenic into the aquatic environment (Herbel and Fendorf, 2006; Tufano et al., 2008). Under strongly reducing conditions in the presence of sulfide, arsenic concentration in the aqueous phase is controlled by the formation of insoluble arsenic-sulfide species (Harvey et al., 2002; Ryu et al., 2002).

The behavior of antimony in natural waters has received less attention than that of arsenic (Filella et al., 2002, 2009; Wilson et al., 2010). The mobility of antimony depends on its oxidation state, nature of substrates available for adsorption, and composition of the aqueous matrix. The Sb(III) species adsorbs strongly to Fe- and Mn-(hydr)oxides over a wide pH range (Belzile et al., 2001; Filella et al., 2002; Leuz et al., 2006a; Casiot et al., 2007; Wilson et al., 2010). In laboratory studies, Sb(V) has been shown to adsorb effectively to Fe-(hydr)oxides (e.g. Tighe et al., 2005; Leuz et al., 2006a, 2006b), Mn-(hydr)oxides, and clay minerals (Xi et al., 2010, 2011; Ilgen and Trainor, 2012). In natural soils, Sb(V) has been found to be predominantly associated with Fe-oxides (Scheinost et al., 2006). Tighe et al. (2005) investigated Sb(V) sorption by amorphous $Fe(OH)_3$ and floodplain soils across a pH range of 2.5–7; adsorption was found to decrease with increasing pH, with maximum sorption occurring at approximately pH 4. Similar results have been observed with Sb(V) adsorption to goethite, whereas Sb(III) strongly adsorbed over a pH range of 3–12 (Leuz et al., 2006a). It has also been observed that Sb(III) adsorbed to goethite can be oxidized (Leuz et al., 2006a), which suggests that sorption is a potentially important pathway promoting oxidation (Mason et al., 2012). A number of additional studies support the findings that iron (hydr)oxides are important sorbents for Sb(V) in near surface environments (Mitsunobu et al., 2006; Scheinost et al., 2006; Ackermann et al., 2009). However, the incorporation of oxidized antimony into secondary Sb–Fe or Sb–Ca co-precipitates (Klimko et al., 2011) immediately adjacent to the weathering sulfide sources may have a significant impact on downstream speciation.

In the present study, we compare the geochemical behavior of antimony and arsenic in two drainage systems within Denali National Park and Preserve, Alaska, both of which are impacted by historic antimony mining operations. Based on the studies summarized above, we expect that the extent of arsenic and antimony transports within the drainages under examination will be strongly influenced by both the redox characteristics of the system and the heterogeneous chemistry associated with solid-phase partitioning. Hence, analysis of arsenic and antimony speciation in the surface water was conducted to correlate oxidation state with transport characteristics along downstream profiles, and the fine-fraction bed sediments were characterized to correlate transport with extent of solid-phase partitioning.

2. Study area

Gold districts with orogenic and intrusion-related lode gold deposits (e.g., Goldfarb et al., 2005) also commonly contain massive stibnite. The stibnite may be present in the gold-bearing lodes, or as distinct antimony-rich veins and pods (Bundtzen, 1978). Quartz and carbonate are the common gangue phases associated with the gold and antimony deposits. Such deposits are particularly common within the Tintina Gold Province (TGP) of interior Alaska and Yukon (Hart et al., 2002), several of which served as a primary source of antimony ore throughout World Wars I and II (Ebbley and Wright, 1948; Bundtzen, 1978).

In the current study, the Kantishna Hills gold and antimony mining district, located within the northwestern part of Denali National Park and Preserve, was investigated (Fig. 1). This district contains a number of antimony lode deposits including Alaska's historically largest antimony producer, the Stampede mine, as well as occurrences along Slate, Caribou, and Eureka Creeks that included the Slate Creek, Last Chance, and Eureka deposits, respectively. Various amounts of antimony were recovered from these deposits starting in the early 20th century through the mid-1980s, totaling roughly 40% of the total antimony produced in Alaska (Bundtzen, 1983; Eppinger et al., 2000).

The Kantishna district is made up of a number of massive northeast trending stibnite- and gold-bearing quartz veins extending over a linear distance of 65 km from Slate Creek in the southwest to Stampede Creek in the northeast (Capps, 1918; Ebbley and Wright, 1948; Bundtzen and Turner, 1979). Pyrite is commonly associated with the stibnite and arsenopyrite, with calcite and other carbonate phases present in low abundances. The host rocks consist of Precambrian to Paleozoic metamorphic rocks of the Birch Creek Schist, the Spruce Creek sequence, and the Keevey Peak and Totatlanika Schists (Davis, 1922; Moffit, 1933; White, 1942; Bundtzen, 1978, 1983, 1994; Bundtzen and Turner, 1979); the main host lithology is schistose quartzite. The veins that make up the bulk of the orebodies in the area are structurally controlled along faults. The veins range in width from 8 cm to >9 m and in length from 30 m to >500 m (Capps, 1918; Lingren, 1933; Bundtzen, 1981; Zobrist et al., 2000). Post-ore fault motion brecciated many of the massive stibnite bodies increasing their susceptibility to later weathering and erosion. Stream and terrace gravels below the known lode systems are sites of extensive placer mining (Salisbury and Dietz, 1984).

Except for some preliminary data in Mueller et al. (2010), no hydrogeochemical data from Stampede Creek are available. Eppinger et al. (2000), however, conducted a reconnaissance level study of the Slate Creek deposit. They sampled undisturbed, but mineralized springs and streams, streams and pools that had contacted waste-rock, and mine tailings and streams downstream of the mined zone. They noted the pH in the waters ranged from 3 to 8, specific conductance ranged from 130 to 1700 μS/cm, and antimony concentrations ranged from <1 μg/L to 190 μg/L. The highest antimony concentrations were found in water within the mine site; however, undisturbed mineralized samples also contained as much as 14 μg/L dissolved antimony. Stream sediments were sampled and revealed a wide range of relatively high antimony concentrations from 43 to 6000 mg/kg.

3. Methods

3.1. Field sampling and in situ measurements

Field sampling was conducted twice at sites along Slate Creek in August 2005 and July 2007. The sampling locations are shown in Fig. 2 and sample descriptions are given in Table 1. In 2005, water and bed-sediment samples were collected, whereas only water samples were collected in 2007. Slate Creek merges with Eldorado Creek and, later, with Moose Creek (Fig. 2). For simplicity, all waters potentially influenced by Slate Creek mine-drainage are referred to as the “main drainage”. In 2005 a sample was collected upstream of any visual mine disturbance (background sample 05SC01), within and downstream of the mine workings, as well as from a waste pile seep (05SC02) and other minor tributaries. A pond immediately adjacent to the main drainage (05SC16) and two springs flowing from the embankment into the main drainage (05SC14A/B) were also sampled.

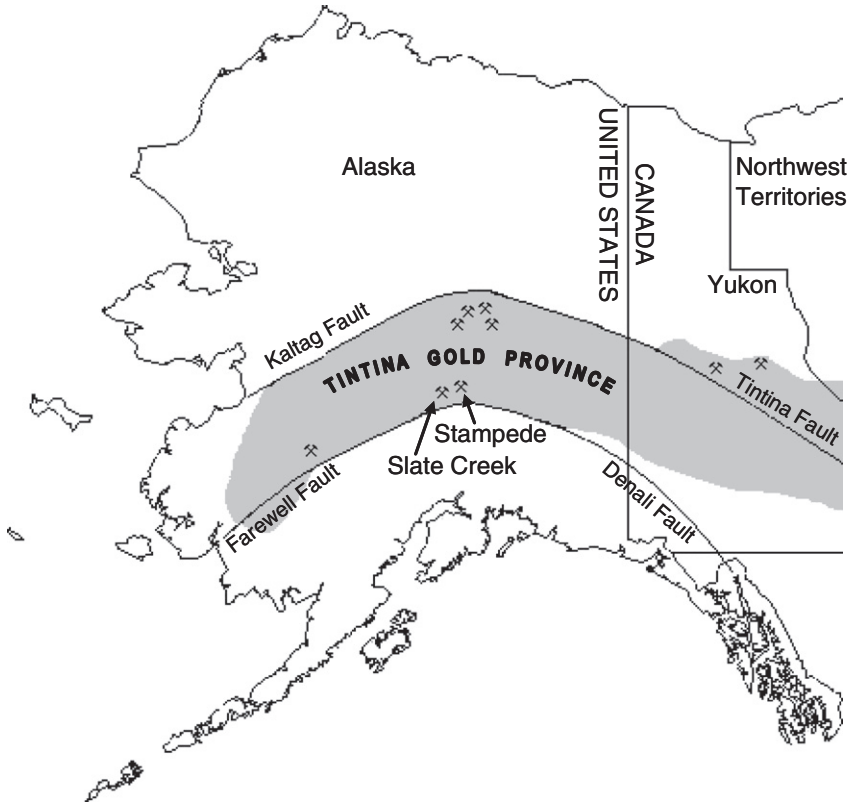

Fig. 1. Map outlining the Tintina Gold Province (shaded area), major faults, and the Stampede Creek and Slate Creek study areas. Modified from Eppinger et al. (2000).

One sample was collected from Moose Creek (05SC21) downstream of the confluence with Slate Creek to further investigate the dilution profile of the mine-affected waters. Although the exact 2005 main drainage locations were not re-sampled in 2007, the same pond (05SC16) and waste pile seep near the headwater (05SC02) were re-sampled as 07SC08 and 07SC03, respectively.

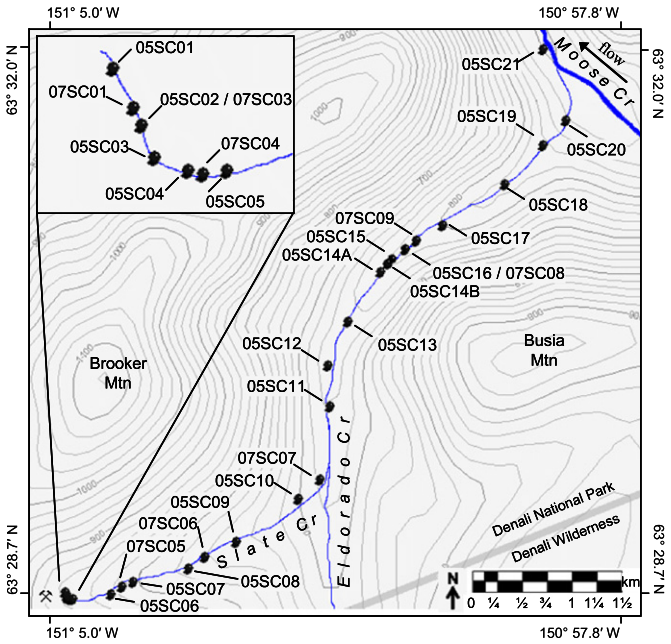

Fig. 2. Slate Creek (2005 and 2007) water and bed-sediment sampling locations. Sample sites with an 05 prefix were collected in 2005 and those with an 07 prefix were collected in 2007.

In 2007, additional samples were collected from Friday (07FR01) and Eureka (07EK01) Creeks (not shown on the site map), which are tributaries to Moose Creek entering from the east side of the drainage. The confluences of Eureka and Friday Creeks with Moose Creek are located ~0.5 km upstream and ~1 km downstream, respectively, from the Slate Creek confluence with Moose Creek. Both Friday and Eureka Creeks have been disturbed by historic placer Au mining (Bundtzen, 1978). Two Moose Creek samples (not shown) were also collected during 2007; one upstream (07MC01) and one downstream (07MC02) of the Slate Creek confluence with Moose Creek. These samples were collected to determine the hydrogeochemical signatures of the mineralized/disturbed drainages.

The Stampede Creek field sampling was conducted in July of 2006 and the sampling locations are shown in Fig. 3. Samples were collected upstream, downstream, and within the mined areas, as well as from minor tributaries. Pore water (06STcore) was collected from a tailings pile within the old mine workings (including a former mill site) that is adjacent to the main drainage. In Fig. 3, site 06ST04 is immediately upstream of the tailings pile, and site 06STCore is in the center of the tailings pile. Two samples (06ST13, 06ST18) were collected upstream and one sample (06ST15) downstream of the Clearwater Fork and Stampede Creek confluence to determine the hydrogeochemical signatures of the Stampede Creek input (Fig. 3).

Water samples from a total of 42 sites were collected in HDPE bottles (HDPE amber bottles were used for arsenic, antimony and iron speciation samples), and filtered in the field using <0.45 μm high capacity Geotech disposable filters. Additional samples were collected at a subset of locations (18 total) by filtering through <0.2 μm pore-size syringe filters to qualitatively determine Sb transport within a defined colloidal-fraction. Water samples were field-preserved by acidification with ultrapure 6 M HNO_3 for major cation and trace metal analyses and with ultrapure 6 M HCl for iron, arsenic, and antimony speciation analyses to pH~2. No preservatives were added to

Table 1
Kantishna Hills sample descriptions and in-situ measurements.

Sample ID	Sample type/location	Dist. from headwater	Cond	pH	Temp	ORP
		km	μS/cm	(±0.5)	°C	mV
05SC01	Slate Cr (~background)	0.00	202	7.5	8.8	–
05SC02	Mine waste seep	0.02	1816	2.8	12.0	–
05SC03	Minor tributary	0.04	512	6.1	10.7	–
05SC04	Slate Cr	0.07	210	7.3	9.6	–
05SC05	Slate Cr	0.10	386	7.3	9.0	–
05SC06	Slate Cr	0.55	393	7.1	10.4	–
05SC07	Slate Cr	0.75	388	7.5	10.1	–
05SC08	Slate Cr	1.35	345	7.5	10.3	–
05SC09	Slate Cr	1.90	339	8.0	9.4	–
05SC10	Slate Cr	2.70	354	8.2	9.9	–
05SC11	Slate Cr	3.90	309	8.0	8.1	–
05SC12	Tributary near tailings	4.49	2710	7.2	8.1	–
05SC13	Eldorado Cr	4.70	334	7.9	6.2	–
05SC14A	Small spring	5.30	2040	6.2	3.3	–
05SC14B	Small spring	5.40	2060	6.1	2.8	–
05SC15	Eldorado Cr	5.50	442	6.8	7.1	–
05SC16	Pond adjacent to Eldorado Cr	5.70	2980	6.3	12.0	–
05SC17	Eldorado Cr	6.10	471	7.6	7.8	–
05SC18	Eldorado Cr	6.80	494	8.1	8.2	–
05SC19	Eldorado Cr	7.30	498	8.1	9.0	–
05SC20	Eldorado Cr	7.70	499	8.3	9.1	–
05SC21	Moose Cr	8.80	286	8.3	8.6	–
06ST01	Stampede Cr (~background)	0.00	838	8.1	3.5	293
06ST02	Stampede Cr	0.40	881	7.9	3.9	–
06ST03	Minor tributary	0.41	727	8.0	3.8	330
06ST04	Stampede Cr	0.69	856	7.9	3.9	334
06STcore	Tailings pore water	0.73	–	2.5	–	–
06ST05	Stampede Cr	0.75	901	7.7	3.8	339
06ST06	Stampede Cr	1.05	961	7.8	4.8	328
06ST07	Stampede Cr	1.10	999	7.7	4.5	187
06ST08	Stampede Cr	1.61	1014	8.1	7.0	322
06ST09	Minor tributary	2.31	521	8.3	11.5	321
06ST10	Stampede Cr	2.49	945	8.2	8.5	327
06ST11	Stampede Cr	3.19	909	8.2	9.8	335
06ST12	Stampede Cr	3.67	894	8.3	10.3	337
06ST13	Clearwater Cr	–	356	8.3	9.1	318
06ST14	Stampede Cr	4.33	522	8.2	6.6	325
06ST15	Clearwater Cr	4.50	420	8.2	8.4	327
06ST16	Unnamed drainage	–	235	7.8	5.1	298
06ST18	Clearwater Cr	–	329	8.2	10.7	312
07SC01	Slate Cr	0.00	237	7.3	4.7	90–100
07SC03	Mine waste seep	0.04	658	5.6	11.0	158
07SC04	Slate Cr	0.10	360	6.6	6.6	120
07SC05	Slate Cr	0.70	432	6.8	7.6	96
07SC06	Slate Cr	1.40	487	7.0	8.3	101
07SC07	Slate Cr	2.90	432	7.8	7.9	189
07SC08	Pond adjacent to Eldorado Cr	5.70	1255	6.2	12.8	228
07SC09	Eldorado Cr	5.75	732	6.8	6.4	124
07EK01	Eureka Cr	–	223	8.1	6.6	155
07MC01	Moose Cr	–	301	8.1	9.0	120
07MC02	Moose Cr	–	345	7.6	9.5	67
07FR01	Friday Cr	–	224	8.3	6.6	168

"–" = not determined, Cond is the conductivity in micro siemens per cm, and ORP is the oxidation reduction potential in milli Volts.

the water samples for alkalinity and anion analyses (0.45 μm filtered). For sulfide analysis, water samples were collected in 125 mL HDPE bottles and field-preserved with 1 mL of 1 M zinc acetate and titrated with 6 N NaOH to pH ≥ 9. Fine-fraction (<63 μm) grab sample

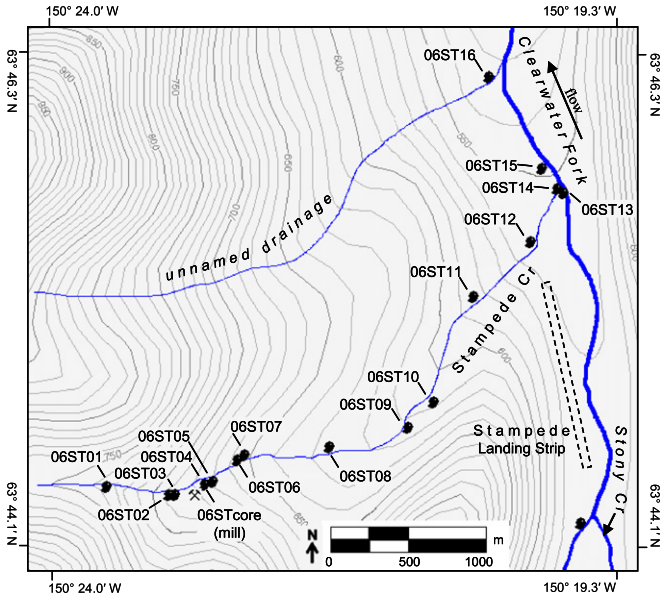

Fig. 3. Stampede Creek (2006) water and bed-sediment sampling locations.

streambed sediments were wet-sieved onsite through polyester screens and collected in HDPE bottles. All samples were stored at 4 °C until analysis.

The oxidation–reduction potential (ORP), pH, conductivity, and temperature were measured in situ (Table 1) using an Oakton Instruments field meter (double junction ORPTestr10, ECTestr high + and pH Testr30). The instrument was calibrated daily using standard solutions.

3.2. Analytical methods

Water samples were analyzed using ion chromatography (Dionex ICS-2000) for major cation (IonPac CS12A column) and anion (IonPac AS19 column) compositions. The operational parameters suggested in the IC column manuals were optimized using standard solutions before sample analysis as described below. The mobile phase for cation analysis was methanesulfonic acid (MSA; supplied by Dionex). To optimize the cation peak resolution, the concentration of MSA was varied from 10 mM at the beginning of the analytical run (0–3 min), to 3 mM (2.5–25 min), followed by a linear increase to 15 mM (26.5–50 min). For the anion analysis, an NaOH (Dionex) mobile phase was used. The optimum peak resolution was observed with the following sequence: 0.5 mM NaOH (0–3 min) linearly increased to 12 mM (3–12 min) and then linearly increased to 50 mM at 12–35 min. The conductivity cell temperature was set at 30 °C. Milli-Q water with a resistivity of 18.2 MΩ·cm, 0.2 μm-filtered and UV-irradiated (<1 μg/L total organic carbon) was used for preparing all solutions (Barnstead NANOpure Diamond).

Minor and trace elements in aqueous samples were measured using an Agilent 7500ce inductively coupled plasma mass spectrometry (ICP-MS) (Creed et al., 1994). To remove $^{40}Ar^{35}Cl$ polyatomic interference during the analysis of arsenic, the ICP-MS was operated in a collision/reaction cell mode using He gas. Streambed sediments were pulverized and digested using a near-total 4 acid (a mixture of hydrochloric, nitric, perchloric, and hydrofluoric acids) digestion method (Briggs and Meier, 2002) and analyzed by ICP-MS (Perkin Elmer ELAN 6000) for major/minor elemental composition.

Alkalinity was determined by titrating 100 mL of a filtered sample with 0.0200 N H_2SO_4 (Fisher) to a pH of 4.5 (Eaton and Franson, 2005). The resulting alkalinity (mg/L $CaCO_3$) was calculated as ten times the volume of 0.0200 N H_2SO_4. For alkalinities <20 mg/L, the titration was stopped in the pH range 4.3 to 4.6, and then continued

using a micro-burette to reduce the pH by 0.3 units. The resulting alkalinity was calculated using the expression (Eaton and Franson, 2005):

$$\mathrm{Alk_{total}, mg\,CaCO_3/L} = \frac{(2B-C)\times N\times 50,000}{\mathrm{mL\ sample}}$$

where B is volume (mL) of H_2SO_4 used to the first recorded pH, C is total volume (mL) of H_2SO_4 to reach pH 0.3 unit lower, and N is normality of H_2SO_4 acid.

The concentration of dissolved sulfide was determined by potentiometric titration (Eaton and Franson, 2005) using a combination silver/sulfide electrode (Orion 94-16). The electrode performance was checked every 2 h and calibration standards were measured every 4 h. The ZnS precipitate formed during sample preservation was separated and dissolved in 50 mL of the alkaline antioxidant reagent and diluted to 100 mL volume with deoxygenated milli-Q water prior to the potential measurement. The alkaline antioxidant reagent was prepared by combining 80 g NaOH, 35 g ascorbic acid ($C_6H_8O_6$), 67 g Na_2H_2EDTA in deoxygenated milli-Q water and bringing the total volume to 1 L.

The oxidation states of arsenic and antimony in water were determined using liquid chromatography (LC; Agilent 1100) coupled to an ICP-MS (Agilent 7500ce). The separation was performed using an arsenic speciation column (Agilent G3154-65001, 4.6 mm × 150 mm i.d.) and guard column (Agilent G3154-65002, 4.6 mm × 10 mm i.d.) packed with chemical bonded hydrophilic anion exchange resin. The mobile phase for arsenic speciation was prepared with 2 mM NaH_2PO_4, 0.2 mM NaEDTA, adjusted to pH 6 with 1 M NaOH, and 50 μg/L Ge as internal standard. Sensitivity optimization was performed at a forward radio-frequency (RF) power of 1400 W, LC injection volume of 50 μg/L, and detector count time of 0.5 s per point (^{75}As) with a total acquisition time of 800 s. The As(III) and As(V) peaks were centered at 112 and 435 s, respectively. The mobile phase for antimony speciation analysis consisted of 12 mM NaEDTA, 2 mM phthalic acid, 3% v/v methanol, 50 μg/L In as internal standard, and the final pH adjusted to 4.5 with 1 M NaOH (modified from Zheng et al., 2000). Sensitivity optimization was performed at a RF power of 1500 W, LC injection volume of 100 μL, and detector count time of 0.5 s per point (^{121}Sb, ^{123}Sb) with a total acquisition time of 450 s. The Sb(III) and Sb(V) peaks were centered at 210 and 130 s, respectively.

The aqueous Fe(II) and Fe_{total} were determined by UV visible spectrophotometry (UV VIS) using the ferrozine method (To et al., 1999). Calibration standards with 0.004–1.6 mg/L of Fe(II) were prepared daily by diluting aliquots of a stock solution (25 mM reagent grade $FeSO_4 \cdot 7H_2O$ in deoxygenated milli-Q water containing 1% v/v ultrapure HCl) in deoxygenated milli-Q water. To prevent oxidation of Fe(II) in standard solutions, and to reduce Fe(III) to Fe(II) in samples intended for the Fe_{total} measurements, a 1 mL aliquot of reagent grade 10% w/v hydroxylamine hydrochloride solution was added to each 40 mL of standard solution or sample in a 50 mL volumetric flask. Then a 1 mL aliquot of 4.9 mM ferrozine reagent was added to all samples, and the total volume of each sample was brought to 50 mL with milli-Q water. The concentration of Fe(II) was determined by measuring the absorbance at 562 nm; Fe(III) was calculated as the difference between Fe_{total} and Fe(II). The Fe_{total} determined using this method was comparable (±5%) to Fe_{total} determined by ICP-MS for all samples. Additional information on analytical methods and site descriptions may be found in Ritchie (2011).

3.3. XAS measurements

To characterize the speciation of arsenic and antimony associated with the solid phases, we utilized X-ray absorption spectroscopy (XAS) in both near edge (XANES) and extended (EXAFS) regions. The XAS data was collected at sector 13 (GSECARS) of the Advanced Photon Source (APS), Argonne National Laboratory on a bending magnet line using a Si(111) water-cooled monochromator. Arsenic K-edge (11,867 eV) and antimony K-edge (30,491 eV) spectra were collected under ambient temperature using a Canberra 16 element Ge detector (in fluorescence mode). For arsenic measurements, a vertical focusing mirror was used to reject higher harmonics. Due to the high energy of the antimony K-edge (30,491 eV), an unfocused X-ray beam was used; for harmonic rejection, the monochromator was detuned by ~50%. Energy calibration was done using Sb- and Au-containing foils. The monochromator step size was 5 eV in the pre-edge, 0.5 eV in the XANES region, and 0.05 $Å^{-1}$ in the EXAFS region with a counting time of 2 s per point. Standards for arsenic oxidation states were sodium meta-arsenite ($NaAsO_2$) and sodium arsenate ($Na_2HAsO_4\ 7H_2O$). Standards for antimony oxidation states were $SbCl_3$ and $KSb(OH)_6$. Standards were scanned in transmission mode.

3.3.1. XAS data analysis

The oxidation state of arsenic in the sediment samples was determined using linear combination fitting (LCF) of sample XANES spectra with the two model compounds (sodium meta-arsenite and sodium arsenate) as end members. At the antimony K-edge energy (30,491 eV) the monochromatic resolution was poor due to the small angular step sizes, therefore the antimony oxidation states were inferred from analysis of first shell Sb–O coordination based on fitting of the EXAFS data. Antimony +3 and +5 exist as oxyanions in surface aqueous systems, and have different coordination with respect to first neighbor oxygen atoms. Antimony (III) has a trigonal pyramidal coordination, whereas Sb(V) is octahedrally coordinated (e.g., Scheinost et al., 2006). The Sb EXAFS data processing and fitting were done using the Athena and Artemis interface (Ravel and Newville, 2005) to the IFEFFIT program (Newville, 2001). Data were normalized, converted into k-space, and background subtracted as described elsewhere (Kelly et al., 2008). The Sb K-edge EXAFS spectra were analyzed by fitting theoretical calculated single scattering (SS) paths. To calculate the theoretical phase and amplitude functions for Sb–O, Sb–S, Sb–Sb, and Sb–Fe SS paths, we used the FEFF6 code (Zabinsky et al., 1995) and known structures of tripuhyite $FeSbO_4$ (Basso et al., 2003) and stibnite Sb_2S_3 (Kyono et al., 2002). The data fitting was performed for k-weights of 1, 2 and 3 simultaneously to ensure that the theory and data exhibit the same k-dependence.

4. Results and discussion

The correlation between antimony and arsenic in stream water and sediment samples from the present study, as well as other samples collected within the Tintina Gold Province (TGP) (Mueller et al., 2010), is shown in Fig. 4. There is a significant correlation between antimony and arsenic concentrations in bed-sediments, and perhaps to a lesser extent between antimony and arsenic in water. The median antimony concentrations of the aqueous and sediment samples appear to be elevated at the Kantishna Hills sites relative to other TGP sites.

In the present study, we have focused on characterizing the hydrogeochemical setting associated with the Kantishna area samples. The in situ conductivity, pH, temperature, and ORP measurements in water from the Kantishna Hills sites are presented in Table 1. The lowest pH values were measured in waters directly derived from mine waste; pH 2.5 in pulverized ore pore water (06STcore) at the Stampede mine site and pH 2.8 in a mine waste seep (05SC02) at Slate Creek. All stream water samples had circum-neutral pH. Conductivities ranged from 512 to 2980 μS/cm in water samples from minor tributaries and 202 to 1014 μS/cm in the main drainage samples. Similar pH and conductivity values for Slate Creek waters were reported by Eppinger et al. (2000).

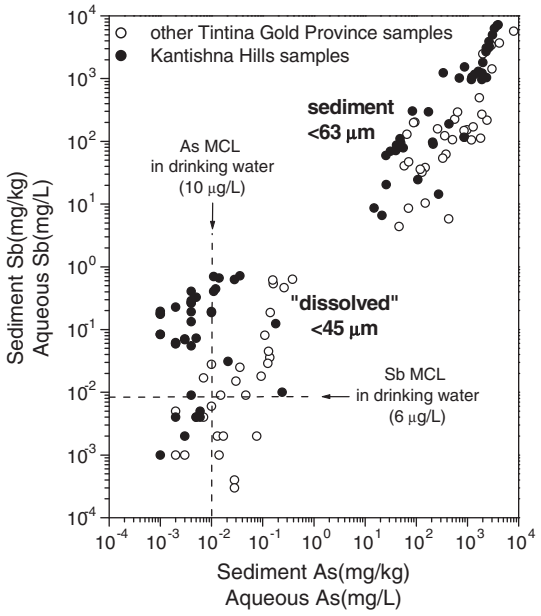

Fig. 4. Correlation between antimony and arsenic concentrations in water and bed-sediments collected from streams draining legacy mining operations in the Tintina Gold Province, including the Kantishna Hills district.
From Mueller et al. (2010).

4.1. Major/minor element aqueous chemistry

The major and minor element compositions of water samples are presented in Table 2. The main drainage and minor tributaries ranged from bicarbonate- to sulfate-dominant in major anion composition (Fig. 5). The more sulfate-dominant waters correspond to samples collected within the mine workings, whereas the more bicarbonate-dominant waters were collected upstream of the mined areas or downstream beyond evident disturbance. The notable exceptions in anion composition are the springs (05SC14A, 05SC14B), pond (05SC16), and mine waste seep (05SC02) samples. The chloride concentrations of the springs and pond samples are higher than stream samples, which suggests a significant degree of volume reduction due to (e.g.) evapotranspiration (Langmuir, 1997). In addition, the alkalinities (in mg/L $CaCO_3$) of the springs and pond samples were below detection (<10 mg/L), although the measured pH values were in the range of 6.1–6.3. This significant lack of buffering capacity is also correlated with a large charge imbalance that indicates an anion component deficiency (Table 2). A rain event was occurring during sampling in 2005, so we speculate that this observation may be attributed to baseflow dilution coupled with an influx of dissolved organic carbon from surface runoff, which is in agreement with previous studies (Buffam et al., 2001; Petrone et al., 2006). The organic acid content was not determined in the samples and, therefore, unaccounted for in charge balance calculations. Conversely, the mine waste seep sample (05SC02) had zero alkalinity; however, this sample was highly acidic (pH 2.8) and sulfate-dominated, consistent with its location in the mine waste pile. Furthermore, this sample indicates a significant cation deficiency that was likely a result of the loss of cations (e.g., Fe^{2+}) associated with rapid oxidation and precipitation during sample collection.

All water samples were calcium–magnesium dominated with respect to major cations (Fig. 5). The highest calcium concentrations were in the spring samples, likely due to longer water–rock interaction of subsurface waters. Similar chemical compositions of Slate Creek waters were reported by Eppinger et al. (2000).

The sum of dissolved base metals, Cd, Co, Cu, Ni, Pb and Zn, is plotted vs. pH in a Ficklin diagram (Fig. 6; after Plumlee et al., 1999). The sum of base metals allows for differentiation between various controls on water composition that would not otherwise be evident from concentration variations in major cations. The designated boundaries in the figure were proposed by Plumlee et al. (1992) for classification of different water types. The waters draining both the Slate Creek and Stampede mineral deposits are classified as near-neutral pH, low base metal waters. The acid water contributions from seeps and other minor tributaries are quickly neutralized/diluted after mixing with the stream waters.

Within the main drainages, calcite ($CaCO_3$) solubility appears to be the primary control on alkalinity. The $CaCO_3$ saturation indices (SI) shown in Fig. 7 were calculated using Visual MINTEQ version 2.32 (Gustafsson, 2005) and the standard MINTEQ thermodynamic database with input analytical totals and in situ pH values from Tables 1 and 2. The results indicate that all main drainage samples, and most from minor tributaries, are close to saturation with respect to calcite (Fig. 7). A mine waste seep (05SC02) was noted to be undersaturated, which is consistent with the lower pH value. Assuming equilibrium with atmospheric CO_2 (35.5 Pa), the low alkalinity spring (05SC14A, 05SC14B) and pond (05SC16) samples are also below saturation. As stated above, this undersaturation with respect to $CaCO_3$ may be due to mixing of $CaCO_3$-rich baseflow with rainwater/surface-runoff.

Calculated SI values indicate approximate saturation to oversaturation with respect to amorphous $Fe(OH)_3$ for all samples (Fig. 7), but undersaturation with respect to Al and Mn mineral and amorphous phases included in the standard MINTEQ database. This is consistent with the observation of iron staining throughout the drainage, particularly near heavily mineralized zones. Several factors may explain the apparent oversaturation, including (i) an incomplete thermodynamic database, (ii) errors associated with tabulated temperature corrections, and (iii) analytical uncertainties caused by the presence of Fe(III) colloids. A comparison of the Fe and Mn contents in the 0.2 μm versus 0.45 μm-filtered samples (Table 3) shows that as much as 23% of total iron and manganese may be associated with colloids ranging in size between the two filter pore sizes. Recalculating the $Fe(OH)_3$ SI using iron total concentrations from the 0.2 μm-filtered samples results in a decrease in SI values (not shown), but still indicates slight oversaturation. Colloidal iron of <0.2 μm-size fraction is also likely contributing to the "dissolved" iron total concentrations, which is supported by previous studies (Kuma et al., 1998; Pullin and Cabaniss, 2003; Bouby et al., 2004; Pokrovsky et al., 2005). Nonetheless, the analytical iron concentrations, calculated SI values, and visual evidence of iron staining all indicate that ferric hydroxides are likely important substrates for sequestration of metal(loids) in this system via sorption and/or co-precipitation processes.

4.2. Aqueous speciation and redox potentials

Aqueous speciation was investigated for the following redox-sensitive elements: S, N, Fe, As, and Sb. Sulfate concentrations ranged from <0.5 to 2115 mg/L (Table 2). Sulfide was below the detection limit (~0.03 mg/L) in all samples. Concentrations of N species (NO_3^-, NO_2^- and NH_4^+) were also below detection in all samples. Total iron concentrations (sum of Fe(II) and Fe(III)) ranged from <12 μg/L to 230 mg/L, with Fe(II)/Fe(III) ratios between 0.1 and 32 (Table 4). Total arsenic concentrations (sum of As(III) and As(V)) in surface and spring waters ranged from <0.3 to 179 μg/L, with As(III)/As(V) ratios between 0.1 and 3. Total As concentration in the pore water extracted from pulverized ore was 3554 μg/L, with an As(III)/As(V) ratio of 78 (Table 4). Concentrations of antimony in surface and spring waters ranged from <1 to 699 μg/L and were 55,000 μg/L in the pore water extracted from pulverized ore (Table 5). The reduced Sb(III) species was below the limit of detection (~5 μg/L) for all samples. Subsequent work has shown that HCl may not be an effective preservative for Sb(III) species (Ilgen et al., 2012), hence the observations of only oxidized species in solution are uncertain.

Table 2
Major and minor element composition of water (0.45 μm-filtered) samples from Kantishna Hills.

Sample ID	Cl^- mg/L (±0.03%)	SO_4^{2-} mg/L (±0.08%)	Alk. as $CaCO_3$ mg/L (±10%)	Na^+ mg/L (±0.72%)	K^+ mg/L (±1.01%)	Mg^{2+} mg/L (±0.42%)	Ca^{2+} mg/L (±0.40%)	Charge balance (%)
05SC01	1.2	28	73.1	0.83	0.26	11.2	22.4	0
05SC02	25	2004	0	0.5	0.62	52.6	69.3	−55
05SC03	22	171	98.0	0.52	0.42	31.9	59.9	−4
05SC04	1.1	34	71.2	0.97	0.31	11.8	23.4	0
05SC05	2.4	89	114	0.85	0.33	30.2	43.4	5
05SC06	3.4	93	104	0.69	0.37	27.7	44.7	5
05SC07	3.4	99	105	0.67	0.34	27.2	45.4	3
05SC08	2.2	85	90.7	0.72	0.38	24.6	41.1	6
05SC09	2.3	89	85.4	0.8	0.34	24.8	40.4	6
05SC10	2.2	90	93.2	0.96	0.38	26.1	42.0	6
05SC11	2.3	57	104	1.4	0.54	18.2	40.6	4
05SC12	55	2115	90.7	4.9	2.7	245	422	−7
05SC13	2.3	73	101	1.4	0.53	19.1	42.8	2
05SC14A	65	224	<10	23.5	2.4	69.1	469	65
05SC14B	100	233	<10	25.1	2.4	70.5	463	59
05SC15	5.3	88	138	2.6	0.57	21.0	62.2	2
05SC16	485	203	<10	139	5.5	187	355	37
05SC17	8.4	93	148	4	0.77	24.8	73.1	6
05SC18	8.4	104	148	3.6	0.75	26.1	71.0	4
05SC19	8.4	106	150	3.6	0.67	23.0	66.3	−1
05SC20	8.6	110	151	3.9	0.73	26.2	77.1	5
05SC21	3	62	77.9	2.9	0.65	12.2	40.4	3
06ST01	6	331	141	0.86	0.95	51.4	108	−1
06ST02	6	342	154	0.99	1.14	56.5	109	−1
06ST03	3.7	290	144	0.85	1.10	54.0	74.5	−5
06ST04	6	336	157	0.94	1.17	57.9	101	−2
06ST05	7.6	354	151	1.02	1.22	63.9	102	−1
06ST06	6	404	174	1.08	1.26	71.3	103	−4
06ST07	5	429	176	1.19	1.36	76.5	106	−4
06ST08	6	448	192	1.33	1.36	77.9	106	−6
06ST09	3.77	117	155	1.08	1.18	27.5	70.4	2
06ST10	6.2	390	157	1.44	1.34	70.4	99.9	−3
06ST11	6	368	156	1.4	1.27	66.5	97.1	−3
06ST12	6.4	362	180	1.46	1.28	65.2	96.1	−5
06ST13	2.6	88	94.5	5.15	0.85	19.0	42.9	2
06ST14	3.5	175	99.4	0.89	0.77	34.7	57.2	0
06ST15	2.6	118	98.0	3.66	0.77	23.4	46.0	−1
06ST16	<0.20	40	77.8	0.92	0.32	11.8	30.7	3
06ST18	2.4	80	87.1	1.25	0.88	14.9	40.0	−3
07SC01	<0.20	32.5	63.1	0.802	0.088	10.4	20.9	0
07SC03	<0.20	144	125	0.636	0.435	30.0	59.6	0
07SC04	<0.20	<0.50	134	0.759	0.122	15.9	27.4	1
07SC05	<0.20	91.2	93.8	0.697	0.204	21.8	35.3	−2
07SC06	<0.20	97.4	103	0.654	0.238	25.0	40.9	1
07SC07	<0.20	73.1	88.0	0.731	0.276	22.2	35.6	5
07SC08	114	65.9	327	28.8	0.842	54.4	103	−1
07SC09	7.71	29.0	288	8.02	0.567	29.2	89.9	5
07EK01	1.27	172	137	1.02	0.564	32.6	70.0	−1
07MC01	1.61	42.7	79.0	3.68	0.460	7.85	32.4	−2
07MC02	2.62	56.3	94.5	3.71	0.624	10.9	41.3	0
07FR01	1.04	151	160	0.967	1.53	28.2	79.0	0

"–" = not determined.

The redox potential (E_H) of water samples was calculated from the analytical data based on two redox couples: Fe(II)/Fe(III) and As(III)/As(V). In Fig. 8, the E_H for the Fe(II)/Fe(III) couple as a function of pH is compared to the theoretical stability fields calculated from thermodynamic data in Langmuir (1997) for a simplified Fe–O_2–H_2O system (10^{-5} M iron [average for Kantishna water samples] at 25 °C and 10^5 Pa). For the majority of the samples, the experimental E_H values fall in the regime expected for aqueous Fe(II) equilibrium with freshly precipitated $Fe(OH)_3$(am). These observations are consistent with relatively slow dissolution of the Fe-bearing primary sulfide minerals (FeS_2, FeAsS) as compared to the equilibration of the Fe(II)/Fe(III) redox couple in oxygenated systems (Stumm and Morgan, 1996; Stefánsson et al., 2005). One exception is the acidic mine waste seep (05SC02, pH 2.8), which is comparatively more reduced than the main drainage and other tributaries, and is apparently undersaturated with respect to amorphous Fe(III) phases. Partial oxidation and precipitation may have occurred during sample collection based on a significant charge imbalance (cation deficiency; Table 2) of the sample, as discussed above. Precipitation would result in a high-biased E_H, so it is possible that the seep waters may be more reduced than calculated.

A similar analysis using the computed E_H values from the dissolved arsenic concentrations suggests that the aqueous As(III) and As(V) species maintain an apparent equilibrium, at least below a pH of about 7, where the $H_2AsO_4^-$ species would be the predominant form of As(V) (Fig. 9). At higher pH values, the $HAsO_4^{2-}$ is the predominant species. The calculated E_H values are above the stability limits for the As-sulfide species and consistent with our observation of the absence of reduced sulfur in the samples.

A comparison of calculated E_H values based on the As(III)/As(V) and Fe(II)/Fe(III) redox couples is presented in Fig. 10. Whereas the

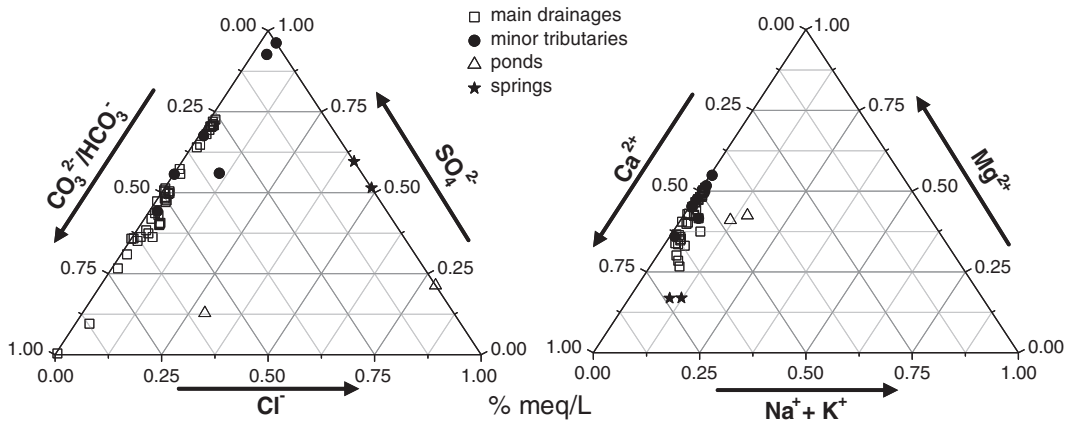

Fig. 5. Ternary diagrams of the major ion components of the water samples from the Kantishna Hills. Tailings and mine waste seep sample are included with the main drainage samples.

correlation is significant, there is an offset between the potentials computed in the two cases (by 0.24 V). These observations are in agreement with previous findings on redox conditions in a cold groundwater (Lindberg and Runnells, 1984) and geothermal waters (Stefánsson and Arnórsson, 2002; Stefánsson et al., 2005). Possible explanations for this commonly observed disequilibrium have been postulated to include improper sample preservation leading to a post-sampling shift in redox species concentrations, variations in tabulated standard E_H^0 data used to calculate E_H (Lindberg and Runnells, 1984) and, as noted above, the inclusion of colloidal iron in the analytical totals leading to overestimation of the E_H values. Nevertheless, the significant correlation leads us to speculate that the arsenic redox chemistry is strongly influenced by the iron chemistry as noted in a number of previous studies (Bednar et al., 2005; Herbel and Fendorf, 2006; Tufano et al., 2008; Weber et al., 2010).

The E_H calculated from the As(III)/As(V) redox couple is also compared to theoretical antimony stability fields (Fig. 9). These computations suggest that the Sb(III)/Sb(V) ratio should be approximately 1 in solution over a wide range of pH. The lack of observed Sb(III) in any of the field samples contradicts this prediction. The reasons for this discrepancy may be due to the inadequacy of HCl as a preservative (Ilgen et al., 2012). However, there is also strong evidence that Sb(III) is highly susceptible to heterogeneous oxidation (Leuz et al., 2006a, 2006b; Mitsunobu et al., 2006; Mason et al., 2012); therefore, it is also plausible that Sb(V) is the dominant solution species which would further imply that the redox behavior of arsenic and antimony is highly distinct. Additional study of this point is warranted.

4.3. Mobility and attenuation of antimony and arsenic

The total antimony and arsenic concentrations in stream water and sediment as a function of distance from headwater (i.e., local background samples) for the 2005 and 2007 Slate Creek, and 2006 Stampede Creek sampling events are shown in Fig. 11a, b, and c, respectively. Both main drainage and minor tributaries are shown, as well as corresponding in situ pH. A listing of antimony and arsenic water and sediment concentrations is provided in Table 5.

As shown in Fig. 11a, there was considerable increase in dissolved antimony and arsenic concentrations within and downstream of the Slate Creek (2005) mine workings compared to concentrations at the headwater (i.e., regional background (05SC01); [Sb] = 4.2 μg/L, [As] = 5.3 μg/L). The antimony and arsenic concentrations in the main drainage increased significantly in the vicinity of the mine waste seep and in another minor tributary flowing from south of the mine disturbance.

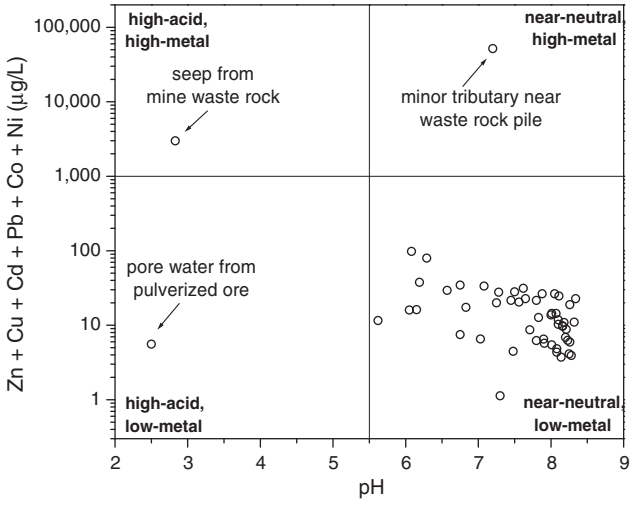

Fig. 6. Ficklin diagram (after Plumlee et al., 1999) showing the sum of dissolved base metals Zn, Cu, Cd, Pb, Co, and Ni as a function of pH in waters draining historic antimony mines in the Kantishna Hills. The designated boundaries were proposed by Plumlee et al. (1992) to classify different drainage compositions.

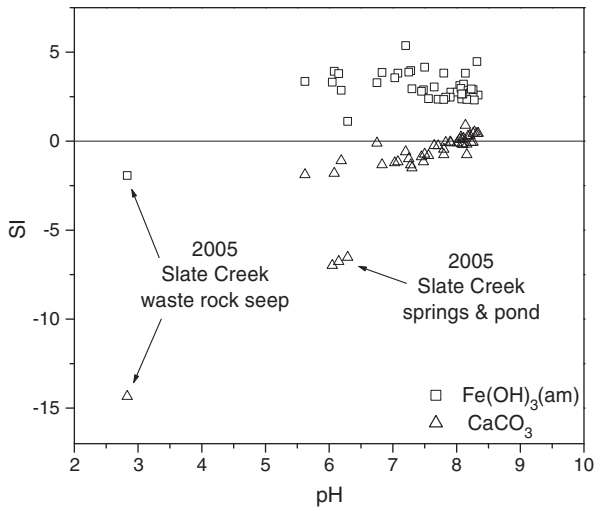

Fig. 7. Calculated saturation indices for calcite ($CaCO_3$) and amorphous ferrihydrite ($Fe(OH)_3$) as a function of pH for the Kantishna Hills mine-drainage and minor tributary waters.

Table 3
Ratios of iron and manganese concentrations of 0.2 μm and 0.45 μm-filtered samples to estimate percent colloidal-fraction in water samples.

Sample ID	[Fe] 0.2 μm/[Fe] 0.45 μm	% colloidal formation	[Mn] 0.2 μm/[Mn] 0.45 μm	% colloidal formation
06ST01	–	–	0.91	9
06ST03	–	–	1.0	0
06ST05	–	–	0.81	19
06ST07	0.91	9	0.99	1
06ST10	–	–	0.85	15
06ST11	–	–	0.77	23
06ST14	0.99	1	0.97	3
06ST16	0.95	5	0.99	1
06ST17	0.95	5	1.0	0
06ST18	–	–	0.95	5
07SC01	0.97	3	1.0	0
07SC03	0.77	23	1.0	0
07SC04	0.80	20	0.98	2
07SC05	0.79	21	1.0	0
07SC06	0.92	8	1.0	0
07SC07	0.84	16	0.89	11
07SC08	0.77	23	0.93	7
07SC09	0.77	23	0.84	16

"–" = not determined.

However, antimony and, to a lesser extent, arsenic concentrations continue to increase downstream of the disturbed mining area, reaching a maximum of 665 μg/L at 0.75 km downstream in the 2005 samples. Antimony concentrations decrease one order of magnitude within another 3 km, but still remain one order of magnitude above (59 μg/L) the EPA MCL (6 μg/L) before merging with Moose Creek ~8 km from the headwater. After merging with Moose Creek, antimony is diluted to <6 μg/L. Dissolved arsenic exceeds the EPA MCL (10 μg/L) by approximately three times at its maximum concentration downstream of the mining disturbance and rapidly decreases to below the MCL within 0.8 km. Further downstream (4.5 km), a significant increase in arsenic concentration (239 μg/L) is due to the input from a minor tributary near an exposed arsenopyrite-rich mine waste pile. However, an increase in dissolved arsenic concentration was not observed 200 m downstream of the confluence due to dilution and/or rapid attenuation via partitioning. A comparison of ratios of $Sb_{water}/Sb_{sediment}$ versus $As_{water}/As_{sediment}$ (from Table 5) reveals that arsenic has a higher relative affinity for sediment partitioning than antimony.

The dissolved antimony and arsenic concentrations from the 2007 Slate Creek sampling event (Fig. 11b) were slightly elevated compared to the 2005 sampling event (Fig. 11a). The lower 2005 observed concentrations are due to larger dilution; stream water levels were higher in 2005 compared to 2007. The higher 2005 water levels are presumed to be due to groundwater input as atmospheric precipitation for several weeks prior to sampling was minimal; the 2005 National Atmospheric Deposition Program recorded levels of snow accumulation and spring rain events that were greater in 2005 than in 2007. Although the exact 2005 main drainage locations were not re-sampled in 2007, the same pond (05SC15, 07SC08) and mine waste seep (05SC02, 07SC03) near the headwater were re-sampled and can be directly compared. The 2007 pond had 22% and 4% higher antimony and arsenic concentrations, respectively. This is consistent with the overall higher antimony and arsenic concentrations of the main drainage resulting from lower water levels and thus less dilution. Conversely, the 2005 mine waste seep contained 400% more antimony and 860% more arsenic than in 2007. In addition, the pH of water in 2005 (2.8) was markedly lower than 2007 (5.6). This may be explained by the flushing (a light rain began minutes prior to sampling in 2005) of secondary sulfate salts that may be deposited within the mine waste materials through evaporation. These metal salts can store acid and metal(loid)s in a highly soluble form that dissolve readily during a rainstorm event, resulting in a high influx of acid and metal(loid)s into the drainage system (Nordstrom and Alpers, 1999; Plumlee et al., 1999).

The 2007 antimony and arsenic concentrations in Moose Creek upstream of the Friday, Slate, and Eureka Creek confluences (not shown in Fig. 11b) were both <1 μg/L (07MC01), indicating a lack of substantial antimony and arsenic input upstream (Table 5). The samples from the Friday and Eureka Creeks were collected ~0.8 km upstream from the junction with Moose Creek and contained 1.7 μg/L antimony and 3.5 μg/L arsenic, and 8.9 μg/L antimony and 3.5 μg/L arsenic, respectively. The Moose Creek sample (07MC02) collected ~0.5 km downstream of the Friday Creek confluence (downstream of all drainages with known mineralization) contained 4.3 μg/L antimony and 2.2 μg/L arsenic. The impact from the upstream mining-affected drainages on Moose Creek water quality is minimized mainly through dilution because Moose Creek contains several times the discharge of the three tributaries.

Antimony was detected in Stampede Creek waters (Fig. 11c) at concentrations ~2 times lower than those in the Slate Creek drainage. Elevated antimony concentrations (11 to 16 μg/L) above the presumed background concentration (2.7 μg/L from sample 06ST01) were detected in samples collected upstream of any known disturbance, whereas arsenic concentrations remained <1 μg/L. Pore water collected from the tailings pile along the bank of the main Stampede Creek drainage contained significant antimony (55,000 μg/L) and arsenic (3510 μg/L) concentrations. Similar to the Slate Creek drainage, in Stampede Creek the maximum dissolved antimony concentration (264 μg/L) was detected approximately 0.9 km downstream from the mine site, and remained greater than the MCL (6 μg/L) before merging with the Clearwater Fork ~3.6 km from the mine site (83 μg/L at 4.3 km from headwater). Downstream (150 m) of the confluence with Clearwater Fork, the antimony concentration decreased to 29 μg/L. Conversely, dissolved arsenic just reached the EPA MCL (10 μg/L) in one main drainage sample (06ST07) and quickly attenuated. Clearwater Fork antimony (<2 μg/L) and arsenic (<1 μg/L) concentrations from samples (06ST13, 06ST18) collected upstream of the Stampede Creek confluence were minimal. The unnamed drainage in Fig. 11c contained 12 μg/L antimony and <1 μg/L arsenic (06ST16). It is unknown if the drainage has been affected by historic mining activity or if the antimony detected is a result of natural weathering processes of unrecognized lode occurrences.

Antimony mobility and arsenic mobility in an aerobic aqueous environment are generally moderated by (co)precipitation and/or adsorption with metal (hydr)oxides (Filella et al., 2002; Roddick-Lanzilotta et al., 2002; Smedley and Kinniburgh, 2002; Tighe et al., 2005; Leuz et al., 2006a; Wilson et al., 2010). This is supported in our study by the high concentrations of arsenic and antimony in the <63 μm-size fraction bed-sediment samples downstream of the mining-affected areas (Table 5). If the dissolved concentrations of arsenic and antimony were mainly influenced by equilibrium exchange, in addition to dilution, then we would expect a constant ratio between the sediment and water samples along the downstream profiles, assuming a linear exchange function. The mismatch in the shapes of the water and sediment profiles (for a given element) evident in Fig. 11a and c, therefore, indicates a decoupling between the sediments and the stream waters. In other words, minimal mixing between the sediment and water/suspended particles limits the rate of exchange as has been observed in previous studies (Smith, 1999, and references therein). Antimony and arsenic sediment concentrations in relation to iron sediment concentrations as a function of distance from headwater are shown for Slate Creek and Stampede Creek main drainage samples in Fig. 12. The ratios of antimony and arsenic to iron in the sediments yield similar downstream sediment profiles to that of total antimony and arsenic sediment concentrations. The high sediment concentrations and high arsenic/antimony to iron correlation (not shown) indicate a strong affinity between the metalloids and iron in bed-sediment. This correlation suggests that sorption and (co)precipitation with iron (hydr)oxides are an important pathway for their attenuation, and the heterogeneous chemistry is likely most prevalent close to the source regions. However, as noted above we

Table 4
Oxidation state of As (determined by LC-ICP-MS) and Fe (determined by UV–vis) in 0.45 μm-filtered water samples.

Sample ID	Description	As(III)	As(V)	[As(III)]/[As(V)]	Fe(II)	Fe(III)	[Fe(II)]/[Fe(III)]
		μg/L	μg/L		mg/L	mg/L	
05SC01	Slate Cr (~background)	<1	5.2	–	0.10	0.02	5.3
05SC02	Mine waste seep	14	165	0.1	50	184	0.3
05SC03	Minor tributary	7.8	3.0	2.6	9.0	4.4	2.0
05SC04	Slate Cr	–	–	–	0.34	0.32	1.0
05SC05	Slate Cr	2.5	8.7	0.3	0.66	0.31	2.1
05SC06	Slate Cr	–	–	–	0.91	0.34	2.7
05SC07	Slate Cr	–	–	–	0.52	0.29	1.8
05SC08	Slate Cr	–	–	–	0.08	0.01	5.7
05SC09	Slate Cr	<1	3.4	–	<0.01	<0.01	–
05SC10	Slate Cr	–	–	–	0.01	0.002	6.0
05SC11	Slate Cr	–	–	–	<0.01	<0.01	–
05SC12	Tributary near tailings	–	–	–	27	13.1	2.1
05SC13	Eldorado Cr	–	–	–	<0.01	<0.01	–
05SC14A	Small spring	3.5	3.1	1.2	3.3	3.0	1.1
05SC14B	Small spring	3.1	3.2	0.9	3.4	2.6	1.3
05SC15	Eldorado Cr	<1	2.9	–	–	–	–
05SC16	Pond adjacent to Eldorado	3.9	1.7	2.2	0.05	0.004	13
05SC18	Eldorado Cr	–	–	–	0.03	0.01	2.7
05SC19	Eldorado Cr	–	–	–	0.02	0.009	1.7
05SC20	Eldorado Cr	<1	1.9	–	<0.01	<0.01	–
06ST01	Stampede Cr (~background)	<1	<1	–	0.02	0.003	7.4
06ST02	Stampede Cr	<1	<1	–	<0.01	0.004	–
06ST03	Minor tributary	<1	<1	–	<0.01	0.007	–
06ST04	Stampede Cr	–	–	–	0.02	0.005	3.3
06STcore	Tailings pore water	3509	45	78	–	–	–
06ST05	Stampede Cr	<1	<1	–	<0.01	<0.01	–
06ST06	Stampede Cr	–	–	–	0.03	0.005	5.0
06ST07	Stampede Cr	3.5	7.4	0.5	0.34	0.03	12
06ST08	Stampede Cr	<1	3.3	–	0.04	0.007	4.9
06ST09	Small creek	–	–	–	0.09	0.003	32
06ST10	Stampede Cr	<1	1.9	–	0.03	0.004	7.5
06ST11	Stampede Cr	–	–	–	0.02	0.002	8.8
06ST12	Stampede Cr	–	–	–	<0.01	<0.012	–
06ST13	Clearwater Cr	–	–	–	0.01	0.003	3.6
06ST14	Stampede Cr	<1	1.0	–	0.12	0.010	13
06ST15	Clearwater Cr	–	–	–	0.04	0.004	9.4
06ST16	Unnamed drainage	–	–	–	0.09	0.004	24
06ST18	Clearwater Cr	–	–	–	0.02	0.002	8.5
07SC01	Slate Cr	<1	4.0	–	0.03	0.05	0.7
07SC03	Mine waste seep	8.9	10	0.9	3.0	3.7	0.8
07SC04	Slate Cr	2.3	8.6	0.3	–	–	–
07SC05	Slate Cr	15	19	0.8	0.86	0.88	1.0
07SC06	Slate Cr	2.9	7.2	0.4	0.28	0.26	1.1
07SC07	Slate Cr	<1	4.6	–	0.01	0.09	0.1
07SC08	Pond adjacent to Eldorado	4.5	1.5	3.0	0.70	0.28	2.5
07SC09	Eldorado Cr	<1	4.4	–	0.56	0.34	1.6
07EK01	Eureka Cr	<1	3.5	–	<0.01	<0.01	–
07MC01	Moose Cr	<1	<1	–	<0.01	<0.01	–
07MC02	Moose Cr	<1	2.2	–	0.09	0.05	1.9
07FR01	Friday Cr	<1	3.4	–	<0.01	<0.01	–

"–" = not determined.

observe a general enhancement in the sediment/water partitioning ratio for arsenic over antimony (Table 5), suggesting that antimony is relatively more mobile in these systems.

4.4. Arsenic and antimony aqueous speciation

The predominant form of arsenic in the Slate and Stampede creeks is As(V). The percent of the As(V) species in the main drainage as a function of distance from the headwater is shown in Fig. 13. In each case the fraction of As(V) decreases in the area of exposed mine wastes, but quickly increases to approximate background levels within 1–3 km of the source. The As(III) species was dominant in the tailings pore water (06STcore), a tributary originating from the mined area (05SC03), a spring (05SC14A), and both pond (05SC16, 07SC08) samples (Table 4). Due to the small volume input of these tributaries and the relatively fast, possibly bio-mediated, oxidation of As(III) to As(V) in oxidized waters (Oremland et al., 2001; Bruneel et al., 2003; Saltikov and Newman, 2003), As(V) remains the dominant species in the main drainages. A summary of arsenic speciation in water samples is presented in Table 4.

The predominant form of antimony in all water samples is Sb(V). Antimony originating from pore water of the pulverized ore, and perhaps the slightly reduced environment of the spring and pond, was expected to have detectable concentrations of reduced species, but Sb(III) was not detected in any sample. As we noted above, HCl appears to be an inadequate preservative for the Sb(III)/(V) redox couple. Furthermore, the Sb(III) detection limit (~5 μg/L) was elevated relative to that for Sb(V) (1 μg/L) due to poor peak resolution. The

Table 5
Dissolved (0.45 μm-filtered) and bed-sediment Sb and As concentrations.

Sample ID	Sample type/location	Sb_{water}	$Sb_{sediment}$	As_{water}	$As_{sediment}$
		μg/L	mg/kg	μg/L	mg/kg
05SC01	Slate Cr (~background)	4.2	968	5.3	1900
05SC02	Mine waste seep	124	1040	180	2370
05SC03	Minor tributary	407	116	12	855
05SC04	Slate Cr	192	4990	4.4	3080
05SC05	Slate Cr	193	7230	10	3980
05SC06	Slate Cr	626	7020	28	3820
05SC07	Slate Cr	665	6330	14	3380
05SC08	Slate Cr	407	3890	3.6	2640
05SC09	Slate Cr	289	3070	3.5	2330
05SC10	Slate Cr	269	3260	4.2	2650
05SC11	Slate Cr	134	2680	3.5	2300
05SC12	Tributary near tailings	9.6	223	239	10,100
05SC13	Eldorado Cr	71	1800	3.2	2000
05SC14A	Small spring	<0.3	14	6.9	272
05SC14B	Small spring	<0.3	1530	6.1	875
05SC15	Eldorado Cr	69	1220	3	1920
05SC16	Pond adjacent to Eldorado	3.7	189	5.9	435
05SC17	Eldorado Cr	62	1300	2	1640
05SC18	Eldorado Cr	60	972	2	1190
05SC19	Eldorado Cr	59	1060	2	1220
05SC20	Eldorado Cr	59	1170	2	1380
05SC21	Moose Cr	3.4	25	<1	107
06ST01	Stampede Cr (~background)	2.7	91	<1	214
06ST02	Stampede Cr	11	97	<1	208
06ST03	Minor tributary	20	60	<1	26
06ST04	Stampede Cr	16	79	<1	56
06STcore	Tailings pore water	55,000	–	3509	–
06ST05	Stampede Cr	36	305	<1	84
06ST06	Stampede Cr	175	1240	1	336
06ST07	Stampede Cr	187	1020	10	692
06ST08	Stampede Cr	264	296	3.5	173
06ST09	Minor tributary	4.6	21	<1	26
06ST10	Stampede Cr	228	94	2	50
06ST11	Stampede Cr	196	79	1	44
06ST12	Stampede Cr	180	87	1	41
06ST13	Clearwater Cr	1.9	8.7	<1	15
06ST14	Stampede Cr	83	110	1	48
06ST15	Clearwater Cr	29	70	<1	31
06ST16	Unnamed drainage	12	71	<1	40
06ST18	Clearwater Cr	1.7	6.6	<1	22
07SC01	Slate Cr	55	–	4.4	–
07SC03	Mine waste seep	31	–	21	–
07SC04	Slate Cr	446	–	12	–
07SC05	Slate Cr	720	–	36	–
07SC06	Slate Cr	699	–	11	–
07SC07	Slate Cr	327	–	4.9	–
07SC08	Pond adjacent to Eldorado	4.6	–	6.2	–
07SC09	Eldorado Cr	73	–	4.5	–
07EK01	Eureka Cr	8.9	–	3.5	–
07MC01	Moose Cr	0.63	–	0.6	–
07MC02	Moose Cr	4.3	–	2.2	–
07FR01	Friday Cr	1.7	–	3.5	–

"–" = not determined.

sample preservative (HCl) caused interference with the elution of the Sb(III) species, thus increasing its detection limit. Other studies suggest that Sb(III)/Sb(V) aqueous speciation can be preserved by addition of organic acids, such as lactic, ascorbic, citric, tartaric acids, and EDTA (Filella et al., 2009). Nevertheless, the detection of As(III) species and no Sb(III) may suggest slower oxidation kinetics for As(III) or stabilization via complexation. This observation has been supported in the literature (Leuz et al., 2006b; Mitsunobu et al., 2006).

The behavioral difference of downstream transport of antimony and arsenic can be explained through antimony/arsenic aqueous speciation. In aerobic conditions at mildly acidic to circum-neutral pH, As(V) has a high affinity for mineral surfaces, and arsenic is effectively immobilized by sorption and (co)precipitation with metal (hydr)oxides (Smedley and Kinniburgh, 2002; Bissen and Frimmel, 2003). Conversely, Sb(V) has a lower affinity for mineral surfaces suggesting a greater potential for aqueous transport (Belzile et al., 2001; Filella et al., 2002; Casiot et al., 2007; Wilson et al., 2010). These results are in agreement with previous studies of antimony and arsenic mobility in mining-impacted water (Ashley et al., 2003; Casiot et al., 2005, 2007).

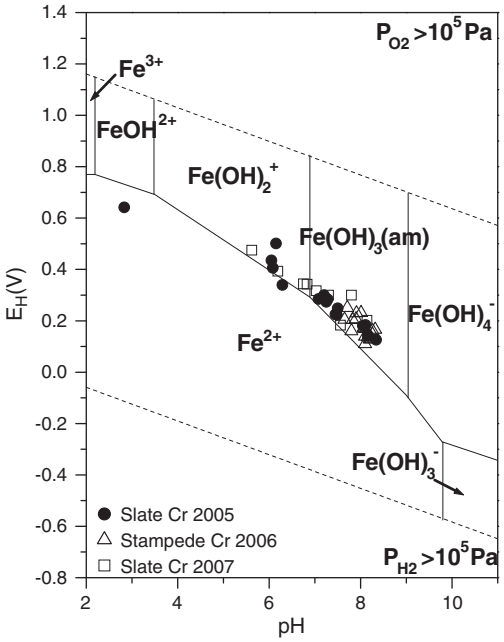

Fig. 8. E_H–pH diagram showing calculated E_H values based on the Fe^{2+}/Fe^{3+} redox couple. The boundaries show stable phases in a simplified Fe–O_2–H_2O system at dissolved concentrations of 10^{-5} M Fe at 25 °C and 10^5 Pa. Thermodynamic data was obtained from Langmuir (1997).

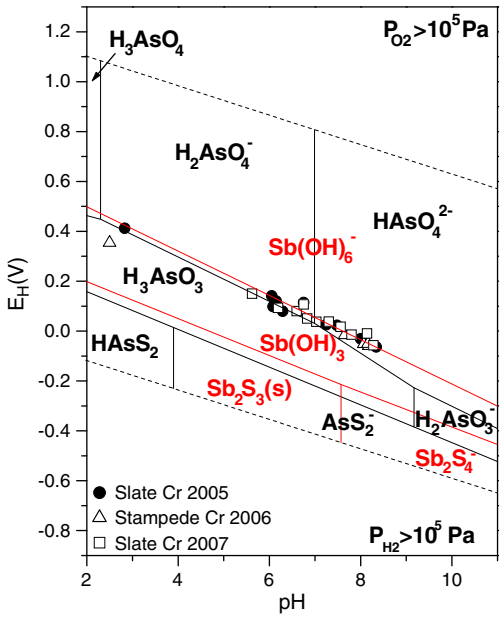

Fig. 9. E_H–pH diagram showing calculated E_H values based on the As(III)/As(V) redox couple. The boundaries (black lines) show stable phases in a simplified As–S–H_2O system at dissolved concentrations of 10^{-6} M As and 10^{-2} M S_{total} at 25 °C and 10^5 Pa. Stable Sb phases (red lines) for a Sb–S–H_2O system (10^{-8} M Sb and 10^{-3} M S at 25 °C and 10^5 Pa) are over-plotted for theoretical comparison. Arsenic thermodynamic data was obtained from Wagman et al. (1982) and Brookins (1988), and antimony data from Ferguson and Gavis (1972) and Vink (1996).

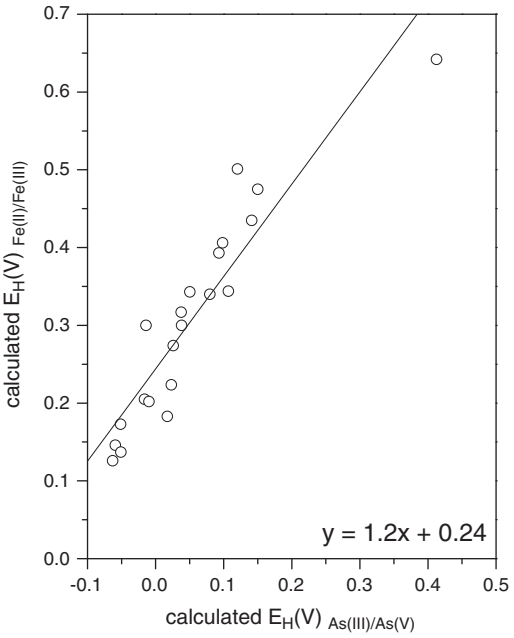

Fig. 10. A comparison of calculated E_H values based on the As(III)/As(V) and Fe(II)/Fe(III) redox couples, in volts (V).

4.5. As and Sb XAS results

Predominantly As(V) was found in the bottom sediments of Slate Creek and Stampede Creek (Table 6). The highest amounts of As(III) were found in the Slate Creek 05SC14B and 05SC16 samples, which are from the downstream spring and pond, respectively. The observation of reduced arsenic in the sediments at these sites correlates with the observation of a relatively high proportion of As(III) in the aqueous phase. The other Slate Creek sites in which As(III) in the sediments was expected based on the aqueous chemistry, are the mine waste seep (05SC02) and minor tributary within the mine waste area (05SC03). However, in both of these samples the majority of sediment arsenic is observed to be As(V). This observation correlates with the relatively high iron content of these waters as compared to waters from sites 05SC14 and 05SC16, suggesting that the greater total iron content of the water has played a role in promoting the oxidation of the sediment-bound arsenic.

The antimony oxidation states inferred from the first shell coordination numbers (CN) suggest that the Slate Creek sediment samples are primarily Sb(V) (Sb–O CN > 5) (Table 7). Of the Slate Creek samples studied, the exception is the sediment from the mineralized spring sample 05SC14B. Based on the EXAFS fitting, the first shell coordination number of 2.8(6) indicates that a significant portion of the antimony in this sample is likely Sb(III) (Table 7). Attempts to include sulfur as the nearest neighbors were not successful, ruling out the presence of sulfide species as contributors to the sediment speciation in this case.

In the Stampede Creek drainage, As(III) was found only in samples from the tailings (Table 6, samples 06STTailings_A, 06STTailings_B, 06STMill_A, 06STMill_B). These samples were collected at different sites within the tailings pile that covers a roughly 20 × 30 m area between the former mill site and Stampede Creek (in Fig. 3, site 06ST04 is immediately upstream of the tailings, and site 06STCore is in the center of the tailings pile). First shell Sb–O CN for the corresponding Sb samples (06STTailings_A, 06STTailings_B, 06STMill_A, 06STMill_B) varies from 1.5(4) to 3.6(5) and indicates that Sb in these samples is also present in reduced Sb(III) form (Table 7). The notable exception within the tailings samples is the Sb–O coordination in sample 06STCoreRed. This sample was taken from a red colored oxidized zone approximately 6 cm below the tailings surface. In this case, the Sb–O CN of 5.5(3) indicates dominantly Sb(V); corresponding arsenic speciation data for this sample is not available. In the downstream samples (06ST07 and 06STBankSed), the predominant form of antimony is Sb(V) (Table 7). The behavior of arsenic and antimony with respect to the sediment oxidation states is relatively consistent within both Slate and Stampede Creek drainages: the more oxidized forms dominate within the (Fe-rich) stream sediments, and only minor amounts of the reduced As(III) and Sb(III) species are found outside of the tailings environment. Within the tailing materials both Sb(III) and As(III) are present.

A more detailed analysis of the Sb EXAFS data for select samples is presented in Table 7 and Fig. 14. The Stampede Creek tailings (sample 06STTailings_B) is a mixture of antimony oxide and antimony sulfide species based on the observation of both S and O in the 1st coordination shell of the EXAFS spectra (Table 7 and Fig. 14). There are also 2 second shell features at ~3.2 and 3.7 Å (uncorrected) distance, which were fitted with S at 3.7 and 3.9 Å respectively; these Sb–S distances are found in the structure of stibnite (Kyono et al., 2002). No evidence of Sb–S backscattering was found in the oxidized tailings sample (06STCoreRed) or in the stream sediments collected downstream from the Stampede tailings (samples 06ST07 and 06STBankSed) or in the Slate Creek stream sediment samples (05SC02, 05SC05, and 05SC07). Based on the shell-by-shell fitting of the EXAFS data for these samples, antimony is predominantly in the oxidized Sb(V) form (CN > 5) and is adsorbed to Fe-oxide solid phase based on the presence of Fe 2nd shell neighbors. The observed Sb–Fe distances of approximately 3.1 Å and 3.6 Å (corrected) for all the oxidized samples indicate two types of adsorption complexes: Sb–Fe bi-dentate edge and Sb–Fe bi-dentate corner-sharing, respectively. These two species are structurally similar to those identified by Scheinost et al. (2006) in shooting range soils. In one sample (06ST07), there is evidence for a mono-dentate complex based on the long Sb–Fe distance (at 4.2 Å corrected). The EXAFS data analysis (Table 7 and Fig. 14) indicates that sediment phase antimony downstream from the sulfide rich zones is oxidized quickly and predominantly present as Sb(V) adsorbed to Fe(III)-oxides. This is in agreement with our interpretation of the aqueous speciation results above; however, it also suggests that whereas Sb(V) may be relatively mobile, relative to Sb(III) or As(III)/(V), it is the predominant species in both the solid and aqueous phase. This points to the important role of oxidation mechanisms and pathways, and again suggests that Sb oxidation is quite rapid in these systems.

5. Summary

Elevated concentrations of antimony and arsenic in both water and stream sediments are associated with historic mining activities along Slate Creek and Stampede Creek within the Kantishna Hills mining district. Background levels of dissolved antimony and arsenic appear to be approximately 4 μg/L and 5 μg/L, respectively, in the Slate Creek drainage. Within the Stampede Creek drainage dissolved background concentrations of arsenic are approximately 2.7 μg/L and ramps up by more than a factor of ten approaching the mineralized areas (but still upstream of any mine development). In Stampede Creek, the background concentrations of arsenic are <1 μg/L. Water quality of both drainage systems is impacted several kilometers downstream from the abandoned mine sites. Dissolved antimony concentrations in Slate Creek exceed the EPA MCL by more than two orders of magnitude near the mine workings and remain one order of magnitude above until the confluence with Moose Creek (~ 8 km from headwater). Dissolved arsenic concentrations also exceed the MCL by ~three times near the mine workings; however, arsenic rapidly decreases to below the MCL within 1.5 km. Similar results are seen for the Stampede Creek drainage, although at slightly lower concentrations.

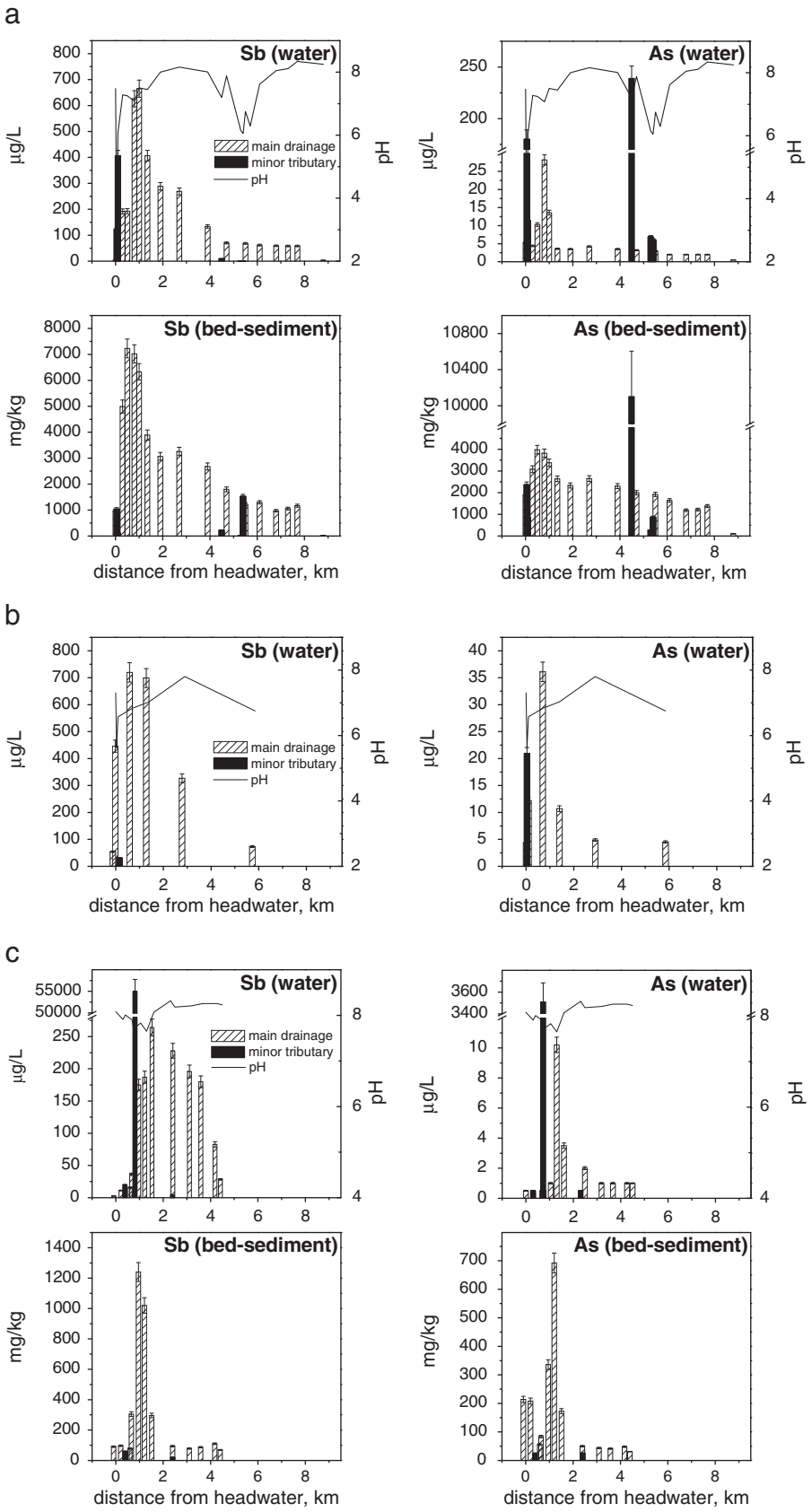

Fig. 11. Total antimony and arsenic concentrations in water and bed-sediment as a function of distance from headwater in (a) Slate Creek 2005, (b) Slate Creek 2007 (water only), and (c) Stampede Creek 2006 samples. Both main drainage (striped bar) and minor tributaries (solid bar), and corresponding pH (line), are plotted.

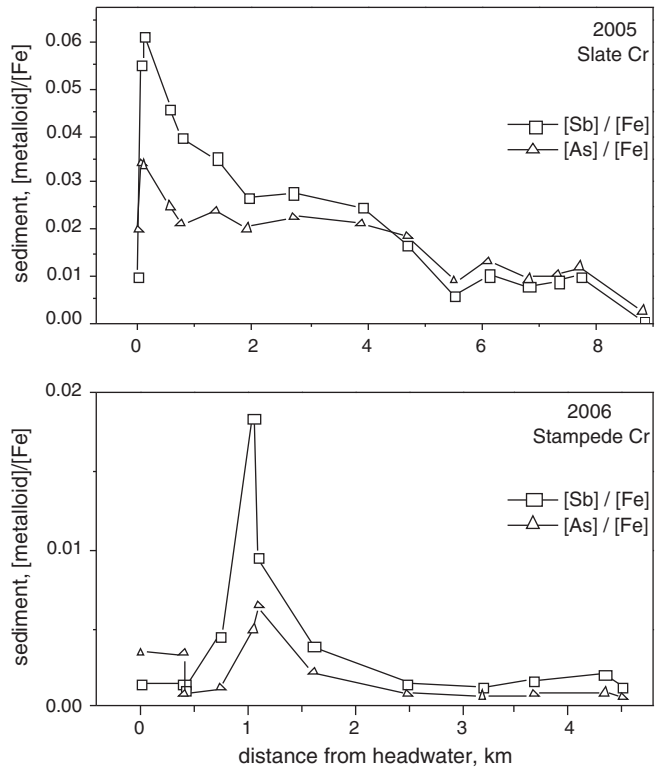

Fig. 12. The ratios of Sb/Fe and As/Fe in sediment with distance from headwater.

The difference between antimony and arsenic transport is attributed to aqueous speciation and different affinities to mineral surfaces, namely iron (hydr)oxides. The predominant form of antimony and arsenic in the main drainage waters is the +5 oxidation state, with As(III) being predominant species in minor tributaries (tailings pore water, pond, and spring samples). Reduced As(III) and Sb(III) were found in mine waste materials, whereas predominantly oxidized forms As(V) and Sb(V) were found in the bottom sediments downstream from the historic mines. The redox potentials calculated from the Fe(II)/Fe(III) and As(III)/As(V) redox couples indicate that the species maintained apparent equilibrium in these waters. Similarly a significant correlation was found in downstream dispersion between antimony/arsenic and iron in the bed-sediment, further indicating the key role iron plays in controlling the mobility of the trace elements.

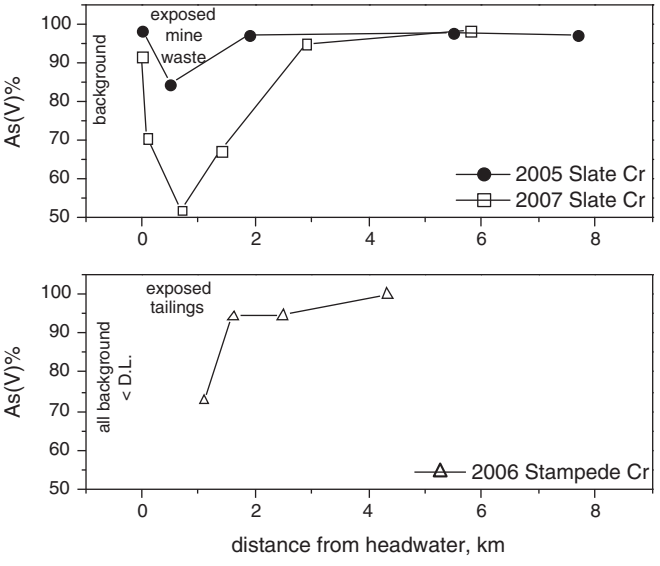

Fig. 13. Percent of As(V) species in main drainage waters as a function of distance from headwater.

Table 6
XAS sediments and tailings sample descriptions and oxidation state of As based on linear combination fitting of XANES spectra.

Sample[a]	Sample description	Fraction As(V) (±0.1)	Fraction As(III) (±0.1)
Slate Creek			
05SC01	<63 μm wet sieved stream sediments	0.9	0.1
05SC02	<63 μm wet sieved stream sediments	1.0	0.0
05SC03	<63 μm wet sieved stream sediments	1.0	0.0
05SC05	<63 μm wet sieved stream sediments	1.0	0.0
05SC06	<63 μm wet sieved stream sediments	0.9	0.1
05SC07	<63 μm wet sieved stream sediments	–	–
05SC09	<63 μm wet sieved stream sediments	0.9	0.1
05SC10	<63 μm wet sieved stream sediments	0.9	0.1
05SC12	<63 μm wet sieved stream sediments	0.9	0.1
05SC14A	<63 μm wet sieved stream sediments	0.9	0.1
05SC14B	<63 μm wet sieved stream sediments	0.3	0.7
05SC16	<63 μm wet sieved stream sediments	0.8	0.2
05SC18	<63 μm wet sieved stream sediments	1.0	0.0
05SC19	<63 μm wet sieved stream sediments	0.9	0.1
05SC20	<63 μm wet sieved stream sediments	0.9	0.1
Stampede Creek			
06ST01	<63 μm wet sieved stream sediments	1.0	0.0
06ST04	<63 μm wet sieved stream sediments	1.0	0.0
06STTailings_A	Main tailings pile, sample A	0.8	0.2
06STTailings_B	Main tailings pile, sample B	0.1	0.9
06STCoreRed	Tailings core sample, red (Fe rich) layer, approx 6 cm below the tailings surface	–	–
06STMill_A	Tailings from the mill site adjacent to the main tailings pile. Surface sample.	0.2	0.8
06STMill_B	Tailings from the mill site adjacent to the main tailings pile. Sub-surface (<5 cm) sample.	0.1	0.9
06ST06	<63 μm wet sieved stream sediments	1.0	0.0
06ST07	<63 μm wet sieved stream sediments	1.0	0.0
06ST08	<63 μm wet sieved stream sediments	1.0	0.0
06STBankSed	Iron rich stream bank sediments	1.0	0.0
06ST10	<63 μm wet sieved stream sediments	1.0	0.0
06ST14	<63 μm wet sieved stream sediments	1.0	0.0

"–" = not determined. The tailings/mill samples are from the same location as 06STCore from Table 1 and Fig. 4.
[a] Samples are listed in downstream orders for each drainage respectively.

Our analysis indicates that the As(V) species is effectively immobilized by sorption or co-precipitation within the oxidized sediments, in agreement with the expected high affinity for mineral surfaces (Herbel and Fendorf, 2006; Courtin-Nomade et al., 2009). The relatively lower affinity of Sb(V) for partitioning to mineral surfaces results in further downstream transport, however, sorption to Fe-(hydr)oxides via an inner-sphere bi-dentate edge and corner sharing complexes appears to be the major attenuation pathway in this system. The observation of sorption controls on Sb(V) mobility, and the coordination chemistry of the adsorption complexes, are similar to previous observations that suggest that sorption to Fe-(hydr)oxides is an important sink for oxidized Sb in soils (Mitsunobu et al., 2006; Scheinost et al., 2006; Ackermann et al., 2009).

Acknowledgments

The authors express gratitude to the National Park Service personnel (Lucy Tyrrell and the late Phil Brease) for access and logistical support; Kunaljeet Tanwar, and Sarah Petitto for field work assistance. We thank Bob Eppinger for a careful review of the manuscript. This research was financially supported by the U.S. Geological Survey Mineral Resources External Research Program grant MRERP-06HQGR0177, National Science Foundation grants CBET-0404400 and CHE-0431425, Strategic Environmental Research and Development Program grant SERDP

Table 7
EXAFS fitting parameters for antimony in Slate and Stampede Creek samples. k-weights of 1, 2, and 3 were fitted simultaneously. Sample descriptions are given in Table 6.

Sample	R-range (Å)	k-range	Shell	N	R (Å)	σ^2	ΔE_0	R-factor	Red χ^2	Indep. Pts	S_0
Slate Creek											
05SC02	1.0–3.8	2.7–10.1	Sb–O	5.4(4)	1.96(1)	0.002(4)	12(1)	0.007	5.9	13	0.87
			Sb-Fe	2(2)	3.57(4)	0.003(6)					
			Sb–Fe	1(1)	3.08(6)	0.004(8)					
05SC05	1.0–3.8	2.7–11.8	Sb–O	5.0(5)	1.97(1)	0.002(1)	−7(2)	0.015	14.8	16	0.87
			Sb–Fe	2(1)	3.55(8)	0.004(5)					
			Sb–Fe	0.8(8)	3.04(7)	0.004(6)					
05SC07	1.0–3.8	2.0–11.7	Sb–O	5.3(3)	1.98(1)	0.003(1)	−3(1)	0.005	7.9	17	0.87
			Sb–Fe	2(1)	3.58(5)	0.006(6)					
			Sb–Fe	1.1(8)	3.11(5)	0.006(6)					
Sb–O shell only fits											
05SC14B	1.0–1.9	2.7–8.6	Sb–O	2.8 (6)	2.0(1)	0.006(3)					0.87
Stampede Creek											
06STTailings_B	1.0–4.0	2.5–12.0	Sb–O	1.4(2)	2.0(2)	0.005(2)	5(3)	0.021	61.3	18	0.87
			Sb–S	1.3(2)	2.52(2)	0.004(5)	8.0(3)				
			Sb–S	0.4(7)	3.7(1)	0.004(12)					
			Sb–S	0.6(6)	3.92(6)	0.005(6)					
06STCoreRed	1.0–4.0	2.4–10.0	Sb–O	6.1(5)	1.97(1)	0.004(1)	7(1)	0.009	37.7	14	0.87
			Sb–Fe	1.7(8)	3.09(4)	0.003(4)					
			Sb–Fe	2(1)	3.56(5)	0.003(5)					
06ST07	1.0–4.0	2.6–12.7	Sb–O	5.5(3)	1.96(1)	0.003(1)	8.3(7)	0.005	10.1	19	0.87
			Sb–Fe	0.4(8)	3.1(1)	0.01(1)					
			Sb–Fe	2(1)	3.55(3)	0.003(2)					
			Sb–Fe	2(2)	4.17(6)	0.003(5)					
06STBankSed	1.0–4.0	2.5–11.7	Sb–O	5.0(3)	1.97(1)	0.002(1)	6.6(8)	0.006	18.5	17	0.87
			Sb–Fe	1.0(5)	3.12(3)	0.003(3)					
			Sb–Fe	1.3(7)	3.56(3)	0.003(4)					
Sb–O shell fits											
06STTailings_A	1.0–2.0	2.6–10.7	Sb–O	3.6(5)	1.98(1)	0.004(2)					0.87
06STMill_A	1.0–2.0	2.5–12.1	Sb–O	2.8(4)	1.97(1)	0.004(2)					0.87
06STMill_B	1.1–2.7	2.6–10.9	Sb–O	1.5(4)	1.96(2)	0.004(4)					0.87

Estimated error of fitted parameters is provided in ().

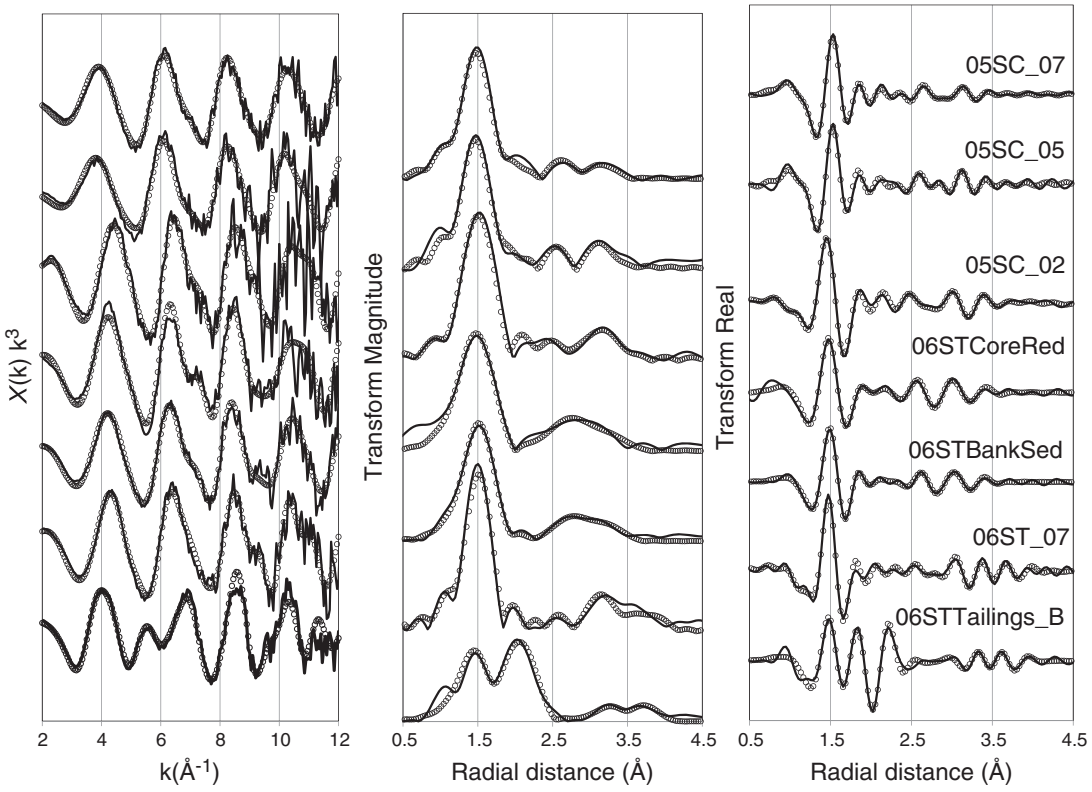

Fig. 14. EXAFS and Fourier Transforms of select Sb samples from the Stampede and Slate Creek drainages. Raw data is shown by the solid lines with corresponding best fits in dotted lines. Fitting parameters are provided in Table 7.

ER-1770, and the Discover Denali Research Fellowship (funded by the National Park Service and the Denali Education Center). Portions of this work were performed at GSECARS (Sector 13), Advanced Photon Source (APS), Argonne National Laboratory. GSECARS is supported by the National Science Foundation (EAR-1128799) and Department of Energy (DE-FG02-94ER14466). Use of the Advanced Photon Source was supported by the U. S. Department of Energy, Office of Science, Office of Basic Energy Sciences, under Contract No. DE-AC02-06CH11357.

References

Ackermann, S., Giere, R., Newville, M., Majzlan, J., 2009. Antimony sinks in the weathering crust of bullets from Swiss shooting ranges. Science of the Total Environment 407 (5), 1669–1682.

Ashley, P.M., Craw, D., Graham, B.P., Chappell, D.A., 2003. Environmental mobility of antimony around mesothermal stibnite deposits, New South Wales, Australia and southern New Zealand. Journal of Geochemical Exploration 77 (1), 1–14.

Basso, R., Cabella, R., Lucchetti, G., Marescotti, P., Martinelli, A., 2003. Structural studies on synthetic and natural Fe–Sb-oxides of MO2 type. Neues Jahrbuch für Mineralogie – Monatshefte 9, 407–420.

Bednar, A.J., Garbarino, J.R., Ranville, J.F., Wildeman, T.R., 2005. Effects of iron on arsenic speciation and redox chemistry in acid mine water. Journal of Geochemical Exploration 85 (2), 55–62.

Belzile, N., Chen, Y.-W., Wang, Z., 2001. Oxidation of antimony(III) by amorphous iron and manganese oxyhydroxides. Chemical Geology 174 (4), 379–387.

Bissen, M., Frimmel, F.H., 2003. Arsenic — a review. Part I: occurrence, toxicity, speciation, mobility. Acta Hydrochimica et Hydrobiologica 31 (1), 9–18.

Bouby, M., Geckeis, H., Manh, T.N., Yun, J.-I., Dardenne, K., Schäfer, T., Walther, C., Kim, J.-I., 2004. Laser-induced breakdown detection combined with asymmetrical flow field-flow fractionation: application to iron oxi/hydroxide colloid characterization. Journal of Chromatography 1040 (1), 97–104.

Briggs, P.H., Meier, A.L., 2002. The determination of forty-two elements in geological materials by inductively coupled plasma-mass spectrometry, chapter. In: Taggart Jr., J.E. (Ed.), Analytical Methods for Chemical Analysis of Geologic and Other Materials, U.S. Geological Survey. Open-File Report 02–223.

Brookins, D.G., 1988. Eh–pH Diagrams for Geochemistry. Springer-Verlag, Berlin, New York, pp. 30–31.

Bruneel, O., Personne, J.-C., Casiot, C., Leblanc, M., Elbaz-Poulichet, F., Mahler, B.J., Le Fleche, A., Grimont, P.A.D., 2003. Mediation of arsenic oxidation by *Thiomonas* sp. in acid mine drainage (Carnoules, France). Journal of Applied Microbiology 95 (3), 492–499.

Buffam, I., Galloway, J.N., Blum, L.K., McGlathery, K.J., 2001. A stormflow/baseflow comparison of dissolved organic matter concentrations and bioavailability in an Appalachian stream. Biogeochemistry 53 (3), 269–306.

Bundtzen, T.K., 1978. A history of mining in the Kantishna Hills. Alaska Journal 8 (2), 150–161.

Bundtzen, T.K., 1981. Geology and mineral deposits of the Kantishna Hills, Mount McKinley quadrangle, Alaska: Fairbanks, Alaska, University of Alaska Fairbanks, 1981 M.S. thesis, pp. 238.

Bundtzen, T.K., 1983. Mineral-resource modeling, Kantishna–Dunkle mine-study areas. Alaska Division of Geological & Geophysical Surveys Report of Investigation 83–1, p. 51.

Bundtzen, T.K., 1994. Kantishna district. In: Plafker, G., Berg, H.C. (Eds.), The Geology of Alaska. The geology of North America, vol. G-1. Geological Society of America, Boulder Colorado, pp. 872–873.

Bundtzen, T.K., Turner, D.L., 1979. Geochronology of metamorphic and igneous rocks in the Kantishna Hills, Mount McKinley quadrangle, Alaska. Alaska Division of Geological & Geophysical Surveys, Short Notes on Alaskan Geology — 1978: Alaska Division of Geological & Geophysical Surveys Geological Report 61F, pp. 25–30.

Capps, S.R., 1918. Mineral resources of the Kantishna region, in: U.S. Geological Survey, Mineral resources of Alaska, report on progress of investigations in 1916. U.S. Geological Survey Bulletin 662, 279–332.

Casiot, C., Lebrun, S., Morin, G., Bruneel, O., Personne, J.C., Elbaz-Poulichet, F., 2005. Sorption and redox processes controlling arsenic fate and transport in a stream impacted by acid mine drainage. Science of the Total Environment 347 (1–3), 122–130.

Casiot, C., Ujevic, M., Munoz, M., Seidel, J.L., Elbaz-Poulichet, F., 2007. Antimony and arsenic mobility in a creek draining an antimony mine abandoned 85 years ago (upper Orb basin, France). Applied Geochemistry 22 (4), 788–798.

Courtin-Nomade, A., Grosbois, C., Marcus, M.A., Fakra, S.C., Beny, J.M., Foster, A.L., 2009. The weathering of a sulfide orebody: speciation and fate of some potential contaminants. The Canadian Mineralogist 47 (3), 493–508.

Creed, J.T., Brockhoff, C.A., Martin, T.D., 1994. EPA Method 200.8, Revision 5.4, Determination of Trace Elements in Waters and Wastes by Inductively Coupled Plasma-Mass Spectrometry. U.S. Environmental Protection Agency. http://water.epa.gov/scitech/methods/cwa/methods_index.cfm.

Davis, J.A., 1922. The Kantishna Region. Alaska Territorial Department of Mines Miscellaneous Report, MR-66-0, p. 85.

Eaton, A.D., Franson, M.A.H., 2005. Standard Methods for the Examination of Water & Wastewater, 21st Centennial edition. Amer. Public Health Assn., Washington D.C.

Ebbley Jr., N., Wright, W.S., 1948. Antimony deposits in Alaska. U.S. Bureau of Mines Report of Investigations 4173, p. 41.

Eppinger, R.G., Briggs, P.H., Crock, J.G., Meier, A.L., Sutley, S.J., Theodorakos, P.M., 2000. Environmental–geochemical study of the Slate Creek antimony deposit, Kantishna Hills, Denali National Park and Preserve, Alaska. Studies by the U.S. Geological Survey in Alaska, 2000: U.S Geological Survey Professional Paper, 1662.

Ferguson, J.F., Gavis, J., 1972. A review of the arsenic cycle in natural waters. Water Research 6 (11), 1259–1274.

Filella, M., Belzile, N., Chen, Y.-W., 2002. Antimony in the environment: a review focused on natural waters: II. Relevant solution chemistry. Earth-Science Reviews 59 (1–4), 265–285.

Filella, M., Williams, P., Belzile, N., 2009. Antimony in the environment: knowns and unknowns. Environmental Chemistry 6 (2), 95–105.

Goldfarb, R.J., Baker, T., Dube, B., Groves, D.I., Hart, C.J.R., Gosselin, P., 2005. Distribution, character and genesis of gold deposits in metamorphic terrains. 100th Anniversary Volume of Economic Geology, pp. 407–450.

Guo, T., DeLaune, R.D., Patrick Jr., W.H., 1997. The influence of sediment redox chemistry on chemically active forms of arsenic, cadmium, chromium, and zinc in estuarine sediment. Environmental International 23 (3), 305–316.

Gustafsson, J.P., 2005. Visual Mineq Version 2.32. KTH. Royal Institute of Technology, Sweden. http://www2.lwr.kth.se/English/OurSoftware/vminteq/.

Hart, C.J.R., McCoy, D.T., Goldfarb, R.J., Smith, M., Roberts, P., Hulstein, R., Bakke, A.A., Bundtzen, T.K., 2002. Geology, exploration, and discovery in the Tintina gold province, Alaska and Yukon. In: Goldfarb, R.J., Nielsen, R.L. (Eds.), Integrated Methods for Discovery, Global Exploration in the Twenty-First Century: Society of Economic Geologists Special Publication, 9, pp. 241–274.

Harvey, C.F., Swartz, C.H., Badruzzaman, A.B.M., Keon-Blute, N., Yu, W., Ali, M.A., Jay, J., Beckie, R., Niedan, V., Brabander, D., Oates, P.M., Ashfaque, K.N., Islam, S., Hemond, H.F., Ahmed, M.F., 2002. Arsenic mobility and groundwater extraction in Bangladesh. Science 298 (5598), 1602–1606.

Herbel, M., Fendorf, S., 2006. Biogeochemical processes controlling the speciation and transport of arsenic within iron coated sands. Chemical Geology 228 (1–3), 16–32.

Ilgen, A., Trainor, T.P., 2012. Sb(III) and Sb(V) sorption onto Al-rich phases: hydrous Al oxide, and the clay minerals kaolinite KGa-1b, oxidized and reduced nontronite NAu-1. Environmental Science and Technology 46, 843–851.

Ilgen, A.G., Foster, A.L., Trainor, T.P., 2012. Role of structural Fe in nontronite NAu-1 and dissolved Fe(II) in redox transformations of arsenic and antimony. Geochimica et Cosmochimica Acta 94, 128–145.

Kelly, S., Hesterberg, D., Ravel, B., 2008. Analysis of soils and minerals using X-ray absorption spectroscopy. In: Ulery, A., Drees, L. (Eds.), Methods of Soil Analysis: Part 5—Mineralogical Methods: SSSA Book Series, no. 5, p. 387.

Klimko, T., Lalinská, B., Majzlan, J., Chovan, M., Kučerová, G., Paul, C., 2011. Chemical composition of weathering products in neutral and acidic mine tailings from stibnite exploitation in Slovakia. Journal of Geosciences 56 (3), 327–340.

Kuma, K., Katsumoto, A., Kawakami, H., Takatori, F., Matsunaga, K., 1998. Spatial variability of Fe(III) hydroxide solubility in the water column of the northern North Pacific Ocean. Deep Sea Research Part I: Oceanographic Research Papers 45 (1), 91–113.

Kyono, A., Kimata, M., Matsuhisa, M., Miyashita, Y., Okamoto, K., 2002. Low-temperature crystal structures of stibnite implying orbital overlap of Sb 5s 2 inert pair electrons. Physics and Chemistry of Minerals 29 (4), 254–260.

Langmuir, D., 1997. Aqueous Environmental Geochemistry. Prentice Hall, Upper Saddle River New Jersey.

Langner, H.W., Inskeep, W.P., 2000. Microbial reduction of arsenate in the presence of ferrihydrite. Environmental Science and Technology 34 (15), 3131–3136.

Leuz, A.-K., Monch, H., Johnson, C.A., 2006a. Sorption of Sb(III) and Sb(V) to goethite: influence on Sb(III) oxidation and mobilization. Environmental Science and Technology 40 (23), 7277–7282.

Leuz, A.-K., Hug, S.J., Wehrli, B., Johnson, C.A., 2006b. Iron-mediated oxidation of antimony(III) by oxygen and hydrogen peroxide compared to arsenic(III) oxidation. Environmental Science and Technology 40 (8), 2565–2571.

Lindberg, R.D., Runnells, D.D., 1984. Ground water redox reactions: an analysis of equilibrium state applied to Eh measurements and geochemical modeling. Science 225 (4665), 925–927.

Lingren, W., 1933. Mineral Deposits, 4th ed. McGraw-Hill, New York.

Mason, S.E., Trainor, T.P., Goffinet, C.J., 2012. DFT study of Sb(III) and Sb(V) adsorption and heterogeneous oxidation on hydrated oxide surfaces. Computational and Theoretical Chemistry 987, 103–114.

Mitsunobu, S., Harada, T., Takahashi, Y., 2006. Comparison of antimony behavior with that of arsenic under various soil redox conditions. Environmental Science and Technology 40 (23), 7270–7276.

Moffit, F.H., 1933. The Kantishna district. U.S. Geological Survey, Mineral Resources of Alaska, Report on Investigations in 1930: U.S. Geological Survey Bulletin, 836-D, pp. 301–388.

Mueller, S.H., Goldfarb, R.J., Farmer, G.L., Sanzolone, R., Adams, M., Theodorakos, P.M., Richmond, S.A., McCleskey, R.B., 2004. Trace, Minor and major Element Data for Ground Water near Fairbanks, Alaska, 1999–2000. U.S. Geological Survey Open-File Report 02–90.

Mueller, S.H., Goldfarb, R.J., Verplanck, P.L., Trainor, T.P., Sanzolone, R.F., Adams, M., 2010. Surface-water, ground-water, and sediment geochemistry of epizonal and shear-hosted mineral deposits in the Tintina Gold Province — arsenic and antimony distribution and mobility. In: Gough, L.P., Day, W.C. (Eds.), Recent U.S. Geological Survey Studies in the Tintina Gold Province, Alaska, United States, and Yukon, Canada—Results of a 5-year Project: U.S. Geological Survey Scientific Investigations Report 2007-5289-G, pp. G1–G9.

Nam, S.-H., Yang, C.-Y., An, Y.-J., 2009. Effects of antimony on aquatic organisms (larva and embryo *Oryzias latipes*, *Moina macrocopa*, *Simocephalus mixtus*, and *Pseudokirchneriella subcapitata*). Chemosphere 75 (7), 889–893.

Newville, M., 2001. IFEFFIT: interactive XAFS analysis and FEFF fitting. Journal of Synchrotron Radiation 8 (2), 322–324.
Nordstrom, D., Alpers, C.N., 1999. Geochemistry of acid mine waters. In: Plumlee, G.S., Logsdon, M.J. (Eds.), The Environmental Geochemistry of Mineral Deposits, Part A: Processes, Methods, and Health Issues. Reviews in Econ. Geol., 6A. Society of Economic Geologists, pp. 133–160.
Oremland, R.S., Newman, D.K., Kail, B.W., Stolz, J.F., 2001. Bacterial respiration of arsenate and its significance in the environment. In: Frankenberger Jr., W.T. (Ed.), Environmental Chemistry of Arsenic. Marcel Dekker, New York, pp. 273–296.
Petrone, K.C., Jones, J.B., Hinzman, L.D., Boone, R.D., 2006. Seasonal export of carbon, nitrogen, and major solutes from Alaskan catchments with discontinuous permafrost. Journal of Geophysical Research 111, G02020.
Plumlee, G.S., Smith, K.S., Ficklin, W.H., Briggs, P.H., 1992. Geological and geochemical controls on the composition of mine drainages and natural drainages in mineralized areas. In: Kharaka, Y.K., Maest, A.S. (Eds.), Low Temperature Environments, v. 1 of Water–Rock Interaction, Proceedings of the 7th International Symposium on Water–Rock Interaction, Park City, Utah, July 13–18, 1992, 1. A.A. Balkema, Rotterdam, pp. 419–422.
Plumlee, G.S., Smith, K.S., Montour, W.R., Ficklin, W.H., Mosier, E.L., 1999. Geologic controls on the composition of natural waters and mine waters draining diverse mineral-deposit types. In: Filipek, L.H., Plumlee, G.S. (Eds.), The Environmental Geochemistry of Mineral Deposits, Part B: Case Studies and Research Topics. Reviews in Econ. Geol., 6B. Society of Economic Geologists, pp. 373–407.
Pokrovsky, O.S., Dupré, B., Schott, J., 2005. Fe-Al-organic colloids control of trace elements in peat soil solutions: results of ultrafiltration and dialysis. Aquatic Geochemistry 11 (3), 241–278.
Pullin, M., Cabaniss, S.E., 2003. The effects of pH, ionic strength, and iron-fulvic acid interactions on the kinetics of non-photochemical iron transformations. I. Iron(II) oxidation and iron(III) colloid formation. Geochimica et Cosmochimica Acta 67 (21), 4067–4077.
Ravel, B., Newville, M., 2005. Athena, Artemis, Hephaestus: data analysis for X-ray absorption spectroscopy using IFEFFIT. Journal of Synchrotron Radiation 12 (4), 537–541.
Ritchie, V.J., 2011. Mobility and chemical fate of antimony and arsenic in historic mining mining environments of Kanthishna Hills, Denali National Park and Preserve, Alaska. University of Alaska Fairbanks, M.S. thesis, pp. 119.
Roddick-Lanzilotta, A.J., McQuillan, A.J., Craw, D., 2002. Infrared spectroscopic characterisation of arsenate (V) ion adsorption from mine waters, Macraes mine, New Zealand. Applied Geochemistry 17 (4), 445–454.
Ryu, J.-H., Gao, S., Dahlgren, R.A., Zierenberg, R.A., 2002. Arsenic distribution, speciation and solubility in shallow groundwater of Owens Dry Lake, California. Geochimica et Cosmochimica Acta 66 (17), 2981–2994.
Salisbury, W.G., Dietz, 1984. 1983 mineral resource studies in the Kantishna Hills & Dunkle mine areas, Denali National Park and Preserve: unpub. report, pp. 234.
Saltikov, C.W., Newman, D.K., 2003. Genetic identification of a respiratory arsenate reductase. Proceedings of the National Academy of Sciences of the United States of America 100 (19), 10983–10988.
Scheinost, A.C., Rossberg, A., Vantelon, D., Xifra, I., Kretzschmar, R., Leuz, A.-K., Funke, H., Johnson, C.A., 2006. Quantitative antimony speciation in shooting-range soils by EXAFS spectroscopy. Geochimica et Cosmochimica Acta 70 (13), 3299–3312.
Smedley, P.L., Kinniburgh, D.G., 2002. A review of the source, behavior and distribution of arsenic in natural waters. Applied Geochemistry 17 (5), 517–568.
Smith, K.S., 1999. Metal sorption on mineral surfaces: an overview with examples relating to mineral deposits. In: Plumlee, G.S., Logsdon, M.J. (Eds.), The Environmental Geochemistry of Mineral Deposits, Part A: Processes, Techniques, and Health Issues. Reviews in Econ. Geol., 6A. Society of Economic Geologists, pp. 161–182.
Smith, K.S., Ficklin, W.H., Plumlee, G.S., Meier, A.L., 1992. Metal and arsenic partitioning between water and suspended sediment at mine-drainage sites in diverse geologic settings. In: Kharaka, Y.K., Maest, A.S. (Eds.), Low Temperature Environments, v. 1 of Water–Rock Interaction, Proceedings of the 7th International Symposium on Water–Rock Interaction, Park City, Utah, July 13–18, 1992, 1. A.A. Balkema, Rotterdam, pp. 443–447.
Smith, K.S., Ficklin, W.H., Plumlee, G.S., Meier, A.L., 1993. Computer simulations of the influence of suspended iron-rich particulates on trace metal-removal from mine-drainage waters. Proceedings of the Mined Land Reclamation Symposium, Billings, Montana., March 21–27, 1993 2, pp. 107–115.
Stefánsson, A., Arnórsson, S., Sveinbjörnsdóttir, A., 2002. Gas pressures and redox reactions in geothermal fluids in Iceland. Chemical Geology 190 (1–4), 251–271.
Stefánsson, A., Arnórsson, S., 2005. Redox reactions and potentials in natural waters at disequilibrium. Chemical Geology 221 (3–4), 289–311.
Stumm, W., Morgan, J.J., 1996. Aquatic Chemistry, 3rd ed. John Wiley and Sons, Inc., New York.
Takahashi, Y., Minamikawa, R., Hattori, K.H., Kurishima, K., Kihou, N., Yuita, K., 2004. Arsenic behavior in paddy fields during the cycle of flooded and non-flooded periods. Environmental Science and Technology 38 (4), 1038–1044.
Tighe, M., Lockwood, P., Wilson, S., 2005. Adsorption of antimony(V) by floodplain soils, amorphous iron(III) hydroxide and humic acid. Journal of Environmental Monitoring 7, 1177–1185.
To, T., Nordstrom, D., Cunningham, K., Ball, J., McCleskey, R., 1999. New method for the direct determination of dissolved Fe(III) concentration in acid mine water. Environmental Science and Technology 33 (5), 807–813.
Tufano, K.J., Reyes, C., Saltikov, C.W., Fendorf, S., 2008. Reductive processes controlling arsenic retention: revealing the relative importance of iron and arsenic reduction. Environmental Science and Technology 42 (22), 8283–8289.
Vaughan, D.J., 2006. Arsenic. Elements 2 (2), 71–75.
Vink, B.W., 1996. Stability relations of antimony and arsenic compounds in the light of revised and extended Eh–pH diagrams. Chemical Geology 130 (1–2), 21–30.
Wagman, D.D., Evans, W.H., Parker, V.B., Schumm, R.H., Halow, I., Bailey, S.M., Churney, K.L., Nuttall, R.L., 1982. The NBS tables of chemical thermodynamic properties: selected values for inorganic and C1 and C2 organic substances in SI units. Journal of Physical and Chemical Reference Data 11 (Suppl. 2).
Weber, F.-A., Hofacker, A.F., Voegelin, A., Kretzschmar, R., 2010. Temperature dependence and coupling of iron and arsenic reduction and release during flooding of a contaminated soil. Environmental Science and Technology 44 (1), 116–122.
White, D.E., 1942. Antimony deposits of the Stampede Creek area, Kantishna district, Alaska. U.S. Geological Survey Bulletin 936-N, 331–348.
Wilson, S.C., Lockwood, P.V., Ashley, P.M., Tighe, M., 2010. The chemistry and behavior of antimony in the soil environment with comparisons to arsenic: a critical review. Environmental Pollution 158 (5), 1169–1181.
Xi, J.H., He, M.C., Lin, C.Y., 2010. Adsorption of antimony (V) on kaolinite as a function of pH, ionic strength and humic acid. Environmental Earth Science 60 (4), 715–722.
Xi, J., He, M., Lin, C., 2011. Adsorption of antimony (III) and antimony (V) on bentonite: kinetics, thermodynamics and anion competition. Microchemical Journal 97 (1), 85–91.
Zabinsky, S., Rehr, J., Ankudinov, A., Albers, R., Eller, M., 1995. Multiple-scattering calculations of X-ray-absorption spectra. Physical Review B: Condensed Matter Materials Physics 52 (4), 2995–3009.
Zheng, J., Ohata, M., Furuta, N., 2000. Antimony speciation in environmental samples by using high-performance liquid chromatography coupled to inductively coupled plasma mass spectrometry. Analytical Sciences 16 (1), 75–80.
Zobrist, J., Dowdle, P.R., Davis, J.A., Oremland, R.S., 2000. Mobilization of arsenite by dissimilatory reduction of adsorbed arsenate. Environmental Science and Technology 34 (22), 4747–4753.